

Synthesis, dielectric properties, molecular docking and ADME studies of pyrrole-3-ones

İrfan Çapan, Mehmet Gümüş, Halil Gökce, Hidayet Çetin, Yusuf Sert & İrfan Koca

To cite this article: İrfan Çapan, Mehmet Gümüş, Halil Gökce, Hidayet Çetin, Yusuf Sert & İrfan Koca (2021): Synthesis, dielectric properties, molecular docking and ADME studies of pyrrole-3-ones, Journal of Biomolecular Structure and Dynamics, DOI: [10.1080/07391102.2021.1914174](https://doi.org/10.1080/07391102.2021.1914174)

To link to this article: <https://doi.org/10.1080/07391102.2021.1914174>

 View supplementary material [↗](#)

 Published online: 23 Apr 2021.

 Submit your article to this journal [↗](#)

 Article views: 55

 View related articles [↗](#)

 View Crossmark data [↗](#)



Synthesis, dielectric properties, molecular docking and ADME studies of pyrrole-3-ones

İrfan Çapan^a , Mehmet Gümüş^{b,c} , Halil Gökçe^d , Hidayet Çetin^e , Yusuf Sert^{e,f}  and İrfan Koca^c 

^aDepartment of Material and Material Processing Technologies, Technical Sciences Vocational College, Gazi University, Ankara, Turkey;

^bAkdağmadeni Health College, Yozgat Bozok University, Yozgat, Turkey; ^cDepartment of Chemistry, Faculty of Art & Sciences, Yozgat Bozok University, Yozgat, Turkey; ^dVocational School of Health Services, Giresun University, Giresun, Turkey; ^eDepartment of Physics, Faculty of Art & Sciences, Yozgat Bozok University, Yozgat, Turkey; ^fSorgun Vocational School, Yozgat Bozok University, Yozgat, Turkey

Communicated by Ramaswamy H. Sarma

ABSTRACT

A novel series of pyrrole-3-one derivatives were synthesized using furan-3-one derivatives and various aromatic amines. The synthesized compounds were identified by spectral studies such as IR, NMR and HRMS. Dielectric properties of the target compounds were experimentally determined by dielectric spectroscopy in the frequency range of 20 Hz – 1 MHz. The real part of the dielectric constant, dielectric loss tangent and conductivity of the samples were investigated as a function of applied frequency. Dielectric measurements showed **Ata7** has the maximum dielectric constant at 1 kHz, while **Ata1** has a negative dielectric constant value. When the result is evaluated with theoretical calculations, grain boundaries play an effective role in the experimental observed dielectric constant. Additionally, in this research the pyrrole-3-one derivatives (**Ata1-9**) were theoretically optimized and over these structures, NMR with GIAO (gauge-independent atomic orbital), UV with TD (time dependent), frontier orbitals (HOMO and LUMO), NLO (nonlinear optical properties) and MEP (molecular electrostatic potential) analysis were carried out. Quantum chemical computations were performed by Density Functional Theory (DFT) using B3LYP functional and 6-311++G (d,p) basis set. Later, the molecular docking analysis between **Ata1-9** and two different receptors such as 3RZE and 3TDA was performed using AutoDock Vina program. Lastly, drug-likeness, physicochemical and ADME/T properties of the designed compounds were computed with the help of SwissADME online tool.

ARTICLE HISTORY

Received 8 February 2021
Accepted 3 April 2021

KEYWORDS

Pyrrole-3-one; dielectric spectroscopy; quantum chemical computations; molecular docking; ADME/T

1. Introduction

Computational chemistry/physics is a branch of chemistry/physics that utilizes computer simulation to help solve chemistry problems with different approach quantum methods. Since molecules are more complicated than atoms, computer programs have been developed to study molecular structure. With these programs, many properties of molecules or reactions can be calculated theoretically. Computer-aided drug design aims to produce a better quality drug in a short time with low cost, with the contributions it makes at the beginning of the classical drug production process. Although molecular docking is a new subject, studies in this area attract a lot of attention. Molecular docking studies play a major role in determining whether or not millions of compounds synthesized are effective. It is impossible to study each of the millions of chemicals individually in vitro and molecular docking studies play a crucial role in selecting of most effective substances. In addition, it prepares the ground for the modification of the molecule with the correct estimation of the binding modes of the relevant molecule and creates a strategic infrastructure for synthesis of molecules that

are likely to be more effective. Considering the recent results, especially in drug design and in the prediction of reaction mechanisms, it can be said that molecular modeling is an essential guide for the experimental chemistry (Frisch, 2009).

Pyrrole is one of the most important simple five membered heterocyclic compounds found in the structure of a wide variety of natural products and pharmaceutical molecules, and is becoming more and more important in materials science (Bhardwaj et al., 2015; Gholap, 2016). Pyrrole derivatives have been displayed a wide spectrum of activities such as antibacterial, antifungal, anti-inflammatory or antitumor. Due to its mentioned properties, pyrrole synthesis is important for scientists (Aksu et al., 2019; Koca & Yildirim, 2012; Qin et al., 2020; Vengatesh et al., 2020). Synthesis and characterization studies of various pyrrol-3-one compounds that were generated from furan-3-ones with amino nucleophiles such as amines, amino acids and antranilic acid derivatives have been reported previously by us and our close colleagues (Koca et al., 2014; Saçmacı et al., 2006; Saçmacı et al., 2005; Üngören et al., 2004). Literature research reveals that compounds close in structure to target compounds have been synthesized so far, but there are no detailed

CONTACT İrfan Koca  i_koca@yahoo.com  Faculty of Arts and Sciences, Department of Chemistry, Yozgat Bozok University, Yozgat, Turkey; Yusuf Sert  yusuf.sert@bozok.edu.tr  Sorgun Vocational School Yozgat, Yozgat Bozok University, Turkey

 Supplemental data for this article can be accessed online at <https://doi.org/10.1080/07391102.2021.1914174>.

© 2021 Informa UK Limited, trading as Taylor & Francis Group

theoretical and molecular docking studies about them. In this study, a number of pyrrole-3-one derivatives were synthesized within the scope of synthesis studies. Aromatic amines with electron-donating and electron-withdrawing groups were used to determine the effect of *N*-substituted groups on the experimental and physical properties of pyrrole-3-one compounds. The structures of the synthesized compounds have been proved by molecular spectroscopic methods.

2. Experimental section

All chemicals and solvents used were obtained from commercial sources and were used as received without further purification. All reactions were viewed by TLC performed on precoated 60 F254 plates (Merck, Whitehouse Station, NJ). Visualization was affected with UV using Camag Thin-Layer Chromatogram Lamp (254/366 nm). Melting points were uncorrected and recorded on Electrothermal 9200 digital melting point apparatus (Yozgat Bozok University). IR spectra were measured with Perkin Elmer Spectrum Two Model FT-IR Spectrophotometer (Yozgat Bozok University) using ATR method with a resolution of 4 cm^{-1} at room temperature and its scan number is 100 and its form is solid phase and region $4000\text{--}400\text{ cm}^{-1}$. The $^1\text{H-NMR}$ spectra were recorded on Bruker 400-MHz spectrometer (Erciyes University) and are reported in ppm (δ) relative to tetramethylsilane (TMS) as the internal standard and $^{13}\text{C-NMR}$ (100 MHz) is referenced to $\text{DMSO-}d_6$. Chemical shifts were reported in ppm (parts per million) values. The data were presented as follows: chemical shift, multiplicity (*s* = singlet, *d* = doublet, *t* = triplet, *q* = quartet, *m* = multiplet, *br* = broad), and coupling constants (*J*) in Hertz (Hz), integration. High-resolution mass spectra data (HRMS) were collected in-house using a Waters LCT Premier XE Mass Spectrometer (high-sensitivity orthogonal acceleration time-of-flight instrument) operating in ESI (+) method, also coupled to an AQUITY Ultra Performance Liquid Chromatography system (Waters Corporation, Milford, MA) (Gazı University). Electrical properties of the samples were investigated by Agilent 4284a, an LCR meter equipped with the software (Yozgat Bozok University). Before electrical measurement, open and short calibration of the LCR meter was performed. The samples were prepared as pellets under the pressure of 10 tons. 16451 B test fixtures were used during the measurement with contact dielectric measurement mode. All the measurements were performed under the atmosphere at room temperature. During the measurement, 0.010 A oscillator current with 1.5 d.c. was applied to the samples.

2.1. General procedure for the synthesis of pyrrole-3-one derivatives

1 mmol corresponding amines was added to furan-3-one compounds (1.0 equiv.) in 1-propanol (30 mL). The mixture was heated at reflux for 6 h. After that, the resulting solution was evaporated under reduced pressure. Diethyl ether was added to the residue to obtain the crude product that is

pale yellow color. The crude product was purified by recrystallization from proper solvents.

2.1.1. Ethyl 2-(1-(4-(dimethylamino)phenyl)-2-hydroxy-4-(4-methoxybenzoyl)-5-(4-methoxyphenyl)-3-oxo-2,3-dihydro-1H-pyrrol-2-yl)acetate (Ata1)

Recrystallized from methanol, Yield 0.382 g, 70%, mp 204°C . $^1\text{H-NMR}$ (400 MHz; $\text{DMSO-}d_6$, ppm): δ 7.83–6.59 (m, 12H, Ar–H), 7.41 (s, 1H, OH), 4.07 (q, 2H, $J = 6.9\text{ Hz}$, OCH_2), 3.84, 3.70 (2 s, 6H, 2 MeO), 2.98 (d, 1H, $J = 16.3\text{ Hz}$, CH_2COOMe , Part A of AB system), 2.87 (s, 6H, $\text{N}(\text{CH}_3)_2$), 2.49 (d, 1H, $J = 16.4\text{ Hz}$, CH_2COOMe , Part B of AB system), 1.15 (t, 3H, $J = 7.1\text{ Hz}$, CH_3). $^{13}\text{C-NMR}$ (100 MHz; $\text{DMSO-}d_6$, ppm): δ 194.5 (CO, ketone), 188.1 (CO, aroyl), 177.5 (CO, ester), 168.7 (N–C=C), 163.0, 161.0, 149.6, 132.4, 132.1, 131.2, 129.4, 124.9, 122.6, 114.0, 113.6, 112.3, 110.7 (C=C), 89.6 (N–C–OH), 60.9 (OCH_2), 55.9, 55.6 (2 \times OCH_3), 40.3 ($\text{N}(\text{CH}_3)_2$), 14.5 (CH_3). **FTIR** (ATR, cm^{-1}): ν 3300 (OH), 3055–2845 (aromatic and aliphatic CH), 1723, 1650, 1623 (C=O), 1607–1463 (C=C, C=N), 1245, 1228 (C–O–C). **HRMS**: *m/z* (*M*+*H*) calcd. for $\text{C}_{31}\text{H}_{32}\text{N}_2\text{O}_7$: 545.224; found: 545.191.

2.1.2. Methyl 2-(1-(4-(dimethylamino)phenyl)-2-hydroxy-4-(4-methoxybenzoyl)-5-(4-methoxyphenyl)-3-oxo-2,3-dihydro-1H-pyrrol-2-yl)acetate (Ata2)

Recrystallized from methanol, Yield 0.402 g, 76%, mp 210°C . $^1\text{H-NMR}$ (400 MHz; $\text{DMSO-}d_6$, ppm): δ 7.82–6.59 (m, 12H, Ar–H), 7.42 (s, 1H, OH), 3.84, 3.71, 3.60 (3 \times s, 9H, 3 \times MeO), 2.99 (d, 1H, $J = 16.4\text{ Hz}$, CH_2COOMe , Part A of AB system), 2.87 (s, 6H, $\text{N}(\text{CH}_3)_2$), 2.50 (d, 1H, $J = 16.4\text{ Hz}$, CH_2COOMe , Part B of AB system). $^{13}\text{C-NMR}$ (100 MHz; $\text{DMSO-}d_6$, ppm): δ 194.5 (CO, ketone), 188.2 (CO, aroyl), 177.5 (CO, ester), 169.2 (N–C=C), 163.0, 16.1, 149.6, 132.4, 132.1, 131.2, 129.4, 124.8, 122.6, 114.0, 113.6, 112.3, 110.6 (C=C), 89.6 (N–C–OH), 55.9, 55.6, 52.2 (3 \times OCH_3), 40.3 ($\text{N}(\text{CH}_3)_2$), 40.1 (CH_2). **FTIR** (ATR, cm^{-1}): ν 3400 (OH), 3075–2840 (aromatic and aliphatic CH), 1735, 1728, 1695, 1646, 1620 (C=O), 1600–1476 (C=C, C=N), 1250 (C–O–C). **HRMS**: *m/z* (*M*+*H*) calcd. for $\text{C}_{30}\text{H}_{30}\text{N}_2\text{O}_7$: 531.209; found: 531.179.

2.1.3. Ethyl 1-(4-(dimethylamino)phenyl)-5-hydroxy-5-(2-methoxy-2-oxoethyl)-2-(4-methoxyphenyl)-4-oxo-4,5-dihydro-1H-pyrrole-3-carboxylate (Ata3)

Recrystallized from 2-propanol, Yield 0.296 g, 63%, mp 206°C . $^1\text{H-NMR}$ (400 MHz; $\text{DMSO-}d_6$, ppm): δ 7.29 (s, 1H, OH), 7.14–6.54 (m, 8H, Ar–H), 3.94 (p, 2H, $J = 7.0\text{ Hz}$, OCH_2), 3.73, 3.55 (2 \times s, 6H, 2 MeO), 2.91 (d, 1H, $J = 16.5\text{ Hz}$, CH_2COOMe , Part A of AB system), 2.85 (s, 6H, $\text{N}(\text{CH}_3)_2$), 2.45 (d, 1H, $J = 16.5\text{ Hz}$, CH_2COOMe , Part B of AB system), 1.01 (t, 3H, $J = 7.1\text{ Hz}$, CH_3). $^{13}\text{C-NMR}$ (100 MHz; $\text{DMSO-}d_6$, ppm): δ 194.1 (CO, ketone), 178.9 (CO, ester), 168.9 (N–C=C), 163.1 (CO, ester), 160.7, 149.7, 130.9, 129.8, 124.2, 123.0, 113.5, 112.1, 100.6 (C=C), 88.9 (N–C–OH), 58.7 (OCH_2), 55.6, 52.1 (2 \times OCH_3), 40.3 ($\text{N}(\text{CH}_3)_2$), 39.5 (CH_2), 14.6 (CH_3). **FTIR** (ATR, cm^{-1}): ν 3390 (OH), 3078–2803 (aromatic and aliphatic CH), 1738, 1714, 1647 (C=O), 1608–1462 (C=C, C=N),

1242–1218 (C–O–C). **HRMS:** m/z (M + H) calcd. for C₂₅H₂₈N₂O₇: 469.193; found: 469.162.

2.1.4. Ethyl 2-(2-hydroxy-4-(4-methoxybenzoyl)-5-(4-methoxyphenyl)-3-oxo-1-phenyl-2,3-dihydro-1H-pyrrol-2-yl)acetate (Ata4)

Recrystallized from 2-propanol, Yield 0.314 g, 63%, mp 158 °C. **¹H-NMR** (400 MHz; DMSO-*d*₆, ppm): δ 7.84–6.80 (m, 13H, Ar–H), 7.54 (s, 1H, OH), 4.04(q, 2H, *J* = 6.9 Hz, OCH₂), 3.84, 3.70 (2s, 6H, 2 MeO), 3.03 (d, 1H, *J* = 16.3 Hz, CH₂COOMe, Part A of AB system), 2.54 (d, 1H, *J* = 16.4 Hz, CH₂COOMe, Part B of AB system), 1.12 (t, 3H, *J* = 7.1 Hz, CH₃). **¹³C-NMR** (100 MHz; DMSO-*d*₆, ppm): δ 194.5 (CO, ketone), 188.3 (CO, aroyl), 177.0 (CO, ester), 168.6 (N–C=C), 163.2, 161.2, 137.2, 132.2, 131.3, 129.5, 128.6, 127.9, 122.2, 114.2, 113.7, 111.7 (C=C), 89.6 (N–C–OH), 61.0 (OCH₂), 55.9, 55.7 (2 × OCH₃), 40.5 (CH₂), 14.4 (CH₃). **FTIR** (ATR, cm^{−1}): ν 3468 (OH), 3065–2837 (aromatic and aliphatic CH), 1724, 1704, 1687, 1615 (C=O), 1600–1475 (C=C, C=N), 1250–1234 (C–O–C). **HRMS:** m/z (M + H) calcd. for C₂₉H₂₇N₂O₇: 502.182; found: 502.179.

2.1.5. Methyl 2-(2-hydroxy-4-(4-methoxybenzoyl)-5-(4-methoxyphenyl)-3-oxo-1-phenyl-2,3-dihydro-1H-pyrrol-2-yl)acetate (Ata5)

Recrystallized from chloroform/cyclohexane, (1:4), Yield 0.342 g, 70%, mp 188 °C (Üngören et al., 2004). **¹H-NMR** (400 MHz; DMSO-*d*₆, ppm): δ 7.85–6.80 (m, 13H, Ar–H), 7.60 (s, 1H, OH), 3.84, 3.70, 3.40 (3 × s, 9H, 3 × MeO), 3.05 (d, 1H, *J* = 16.5 Hz, CH₂COOMe, Part A of AB system), 2.54 (d, 1H, *J* = 16.5 Hz, CH₂COOMe, Part B of AB system). **¹³C-NMR** (100 MHz; DMSO-*d*₆, ppm): δ 194.6 (CO, ketone), 188.4 (CO, aroyl), 176.9 (CO, ester), 169.1 (N–C=C), 163.2, 161.2, 1137.1, 132.1, 132.1, 131.3, 129.5, 128.6, 127.9, 122.2, 114.2, 113.7, 111.6 (C=C), 89.6 (N–C–OH), 55.9, 55.7, 52.2 (3 × OCH₃), 40.2 (CH₂). **FTIR** (ATR, cm^{−1}): ν 3360 (OH), 3074–2838 (aromatic and aliphatic CH), 1728, 1656, 1629, 1607 (C=O), 1600–1463 (C=C, C=N), 1251–1241 (C–O–C). **HRMS:** m/z (M + H) calcd. for C₂₈H₂₅N₂O₇: 488.166; found: 488.160.

2.1.6. Ethyl 5-hydroxy-5-(2-methoxy-2-oxoethyl)-2-(4-methoxyphenyl)-4-oxo-1-phenyl-4,5-dihydro-1H-pyrrole-3-carboxylate (Ata6)

Recrystallized from CCl₄, Yield 0.294 g, 69%, mp 161 °C. **¹H-NMR** (400 MHz; DMSO-*d*₆, ppm): δ 7.48 (s, 1H, OH), 7.31–6.85 (m, 9H, Ar–H), 3.97 (m, 2H, OCH₂), 3.73, 3.38 (2 × s, 6H, 2 MeO), 2.97 (d, 1H, *J* = 16.5 Hz, CH₂COOMe, Part A of AB system), 2.50 (d, 1H, *J* = 16.5 Hz, CH₂COOMe, Part B of AB system), 1.03 (t, 3H, *J* = 7.1 Hz, CH₃). **¹³C-NMR** (100 MHz; DMSO-*d*₆, ppm): δ 194.0 (CO, ketone), 178.6 (CO, ester), 168.8 (N–C=C), 163.0 (CO, ester), 161.0, 136.6, 131.1, 129.4, 129.1, 128.2, 122.6, 113.6, 101.5 (C=C), 89.0 (N–C–OH), 58.9 (OCH₂), 55.7, 52.1 (2 × OCH₃), 39.6 (CH₂), 14.6 (CH₃). **FTIR** (ATR, cm^{−1}): ν 3350 (OH), 3069–2840 (aromatic and aliphatic CH), 1730, 1716, 1648 (C=O), 1603–1440 (C=C, C=N),

1257–1245 (C–O–C). **HRMS:** m/z (M + H) calcd. for C₂₃H₂₃N₂O₇: 426.151; found: 426.148.

2.1.7. Ethyl 2-(1-(4-carbamoylphenyl)-2-hydroxy-4-(4-methoxybenzoyl)-5-(4-methoxyphenyl)-3-oxo-2,3-dihydro-1H-pyrrol-2-yl)acetate (Ata7)

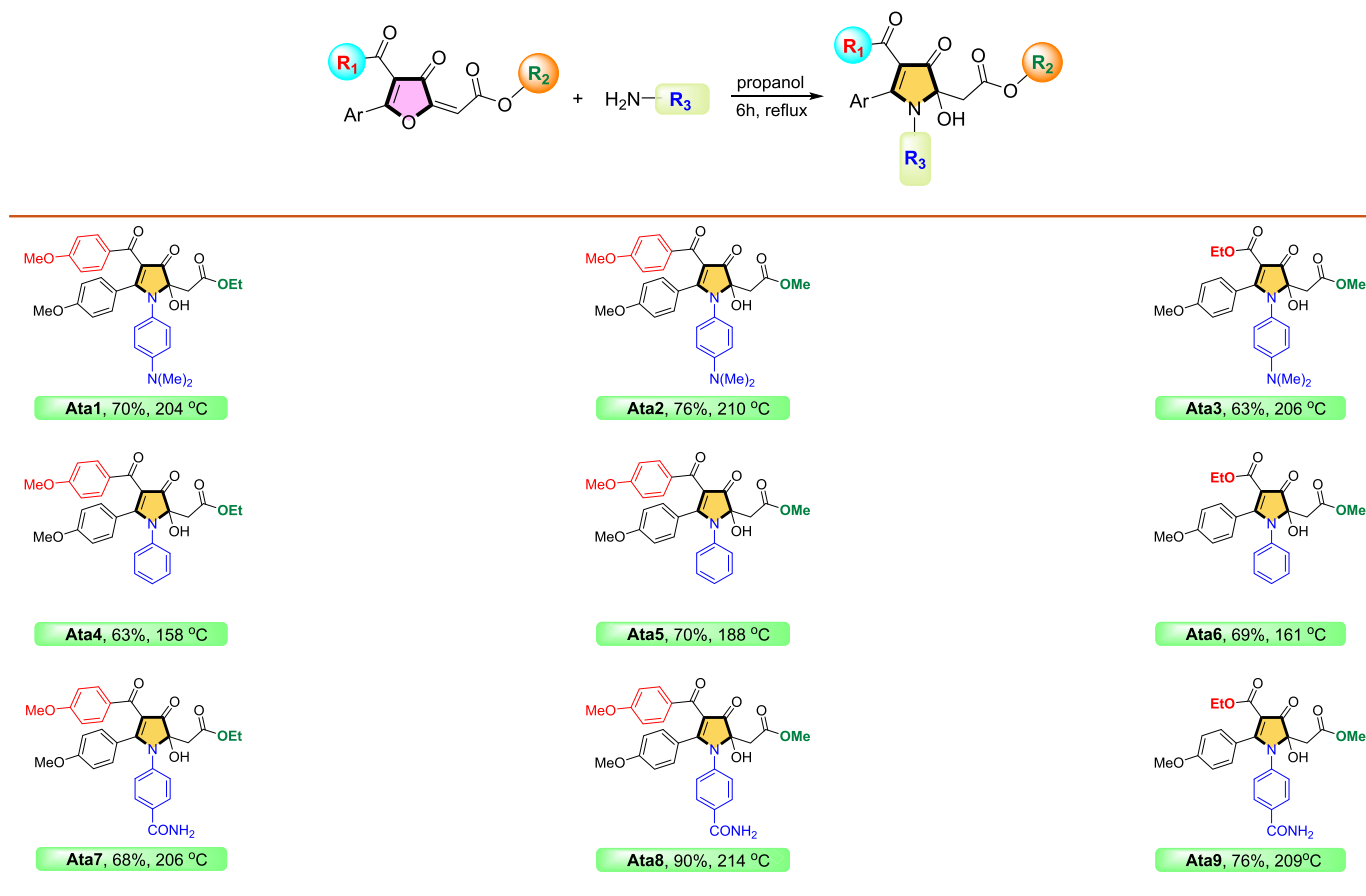
Recrystallized from ethyl acetate, Yield 0.370 g, 68%, mp 206 °C. **¹H-NMR** (400 MHz; DMSO-*d*₆, ppm): δ 7.96 (s, 1H, NH), 7.86–6.83 (m, 12H, Ar–H), 7.65 (s, 1H, OH), 7.41 (s, 1H, NH), 4.03 (q, 2H, OCH₂), 3.84, 3.71 (2 × s, 6H, 2 MeO), 3.06 (d, 1H, *J* = 16.5 Hz, CH₂COOMe, Part A of AB system), 2.59 (d, 1H, *J* = 16.5 Hz, CH₂COOMe, Part B of AB system), 1.11 (t, 3H, *J* = 7.1 Hz, CH₃). **¹³C-NMR** (100 MHz; DMSO-*d*₆, ppm): δ 194.6 (CO, ketone), 188.4 (aroyl), 176.4 (CO, ester), 168.8 (amide), 167.4 (N–C=C), 163.3, 161.4, 140.0, 133.1, 132.2, 132.0, 131.3, 128.7, 127.8, 114.4, 113.8, 112.4 (C=C), 89.7 (N–C–OH), 61.0 (OCH₂), 55.9, 55.7 (2 × OCH₃), 40.6 (CH₂), 14.4 (CH₃). **FTIR** (ATR, cm^{−1}): ν 3415 (OH), 3240–3190 (NH₂), 3070–2840 (aromatic and aliphatic CH), 1728, 1718, 1698, 1667, 1625 (C=O), 1600–1483 (C=C, C=N), 1248 (C–O–C). **HRMS:** m/z (M + H) calcd. for C₃₀H₂₈N₂O₈: 545.224; found: 545.187.

2.1.8. Methyl 2-(1-(4-carbamoylphenyl)-2-hydroxy-4-(4-methoxybenzoyl)-5-(4-methoxyphenyl)-3-oxo-2,3-dihydro-1H-pyrrol-2-yl)acetate (Ata8)

Recrystallized from methanol, Yield 0.478 g, 90%, mp 214 °C. **¹H-NMR** (400 MHz; DMSO-*d*₆, ppm): δ 8.00 (s, 1H, NH), 7.96–6.83 (m, 12H, Ar–H), 7.71 (s, 1H, OH), 7.46 (s, 1H, NH), 3.85, 3.71, 3.56 (3 × s, 9H, 3 MeO), 3.08 (d, 1H, *J* = 16.4 Hz, CH₂COOMe, Part A of AB system), 2.61 (d, 1H, *J* = 16.4 Hz, CH₂COOMe, Part B of AB system). **¹³C-NMR** (100 MHz; DMSO-*d*₆, ppm): δ 194.6 (CO, ketone), 188.4 (CO, aroyl), 176.4 (CO, ester), 169.1 (CO, amide), 167.5 (N–C=C), 163.3, 161.4, 139.9, 133.1, 132.2, 131.3, 128.7, 127.8, 122.0, 114.3, 113.8, 112.3 (C=C), 89.7 (N–C–OH), 56.0, 55.7, 52.3 (3 × OCH₃), 40.3 (CH₂). **FTIR** (ATR, cm^{−1}): ν 3400 (OH), 3334–3311 (NH₂), 3075–2837 (aromatic and aliphatic CH), 1735, 1727, 1696, 1666, 1620 (C=O), 1600–1477 (C=C, C=N), 1250 (C–O–C). **HRMS:** m/z (M + H) calcd. for C₂₉H₂₆N₂O₈: 531.172; found: 531.169.

2.1.9. Ethyl 1-(4-carbamoylphenyl)-5-hydroxy-5-(2-methoxy-2-oxoethyl)-2-(4-methoxyphenyl)-4-oxo-4,5-dihydro-1H-pyrrole-3-carboxylate (Ata9)

Recrystallized from methanol, Yield 0.356 g, 76%, mp 209 °C. **¹H-NMR** (400 MHz; DMSO-*d*₆, ppm): δ 7.98 (s, 1H, NH), 7.76–6.88 (m, 12H, Ar–H), 7.59 (s, 1H, OH), 7.45 (s, 1H, NH), 3.97 (p, 2H, *J* = 7.0 Hz, OCH₂), 3.74, 3.39 (3 × s, 9H, 3 MeO), 2.99 (d, 1H, *J* = 16.5 Hz, CH₂COOMe, Part A of AB system), 2.254 (d, 1H, *J* = 16.4 Hz, CH₂COOMe, Part B of AB system), 1.04 (t, 3H, *J* = 7.0 Hz, CH₃). **¹³C-NMR** (100 MHz; DMSO-*d*₆, ppm): δ 194.0 (CO, ketone), 178.2 (CO, ester), 168.7 (CO, ester), 167.4 (CO, amide), 162.9, 161.2, 139.4, 133.4, 131.2, 128.6, 128.5, 122.3, 113.8, 102.1 (C=C), 89.1 (N–C–OH), 59.1 (OCH₂), 55.7, 52.2 (2 × OCH₃), 39.7 (CH₂), 14.6 (CH₃). **FTIR** (ATR, cm^{−1}): ν 3442 (OH), 3324–3279 (NH₂), 3050–2843 (aromatic and aliphatic CH), 1708, 1683, 1643 (C=O), 1607–1455

Table 1. Synthesis scheme and some properties of compounds **Ata1-9**.

(C=C, C=N), 1257, 1240 (C-O-C). **HRMS:** m/z (M + H) calcd. for $C_{24}H_{24}N_2O_8$: 469.156; found: 469.161.

3. Computational details

The structures of a novel series of pyrrole-3-one derivatives (**Ata1-9**) were optimized to the minimum energy states using the Gaussian 09W package program (Frisch, 2009), DFT/B3LYP method and 6-311++G(d,p) basis set. To NMR calculations, the optimized structures were optimized again in dimethyl sulfoxide (DMSO) solvent. The GIAO approach was used for ^{13}C and 1H -NMR and -NMR chemical shifts and the obtained computational results compared with the experimental NMR data. The theoretical UV-Vis spectral data of the title compounds were calculated by using TD-DFT/B3LYP/6-311++G(d,p) method/basis set in the DMF (*N,N*-dimethylformamide) solvent. Major contributions to electronic transitions in the next step were achieved with the GaussSum 3.0 program (O'boyle et al., 2008). Later section, molecular docking mechanism of **Ata1-9** ligands with two different receptor was obtained with AutoDock Vina software program (Trott & Olson, 2010). In the last section, drug-likeness, physicochemical and ADME/T properties of the designed compounds were calculated with the help of SwissADME and AdmetSAR 2.0 online tools (Yang et al., 2018).

4. Results and discussion

4.1. Synthesis and characterization

The target compounds (**Ata1-9**) were synthesized using furan-3-one derivatives and various aromatic amines (Table 1). For this purpose, three different furan-3-one derivatives were used. Furan-3-ones were prepared through Wittig reaction of corresponding furan-2,3-diones and alkyl 2-(triphenyl- λ^5 -phosphaneylidene)acetate in benzene under reflux condition (Sacmacl et al., 2012; Üngören et al., 2004). The structures of all newly synthesized compounds were ascertained using FTIR, 1H NMR, ^{13}C NMR and mass spectral data.

In this section, spectroscopic characterization will be detailed by interpreting FTIR and NMR analyses with **Ata1** molecule, one of the target compounds synthesized. The FTIR, 1H NMR, ^{13}C NMR and Hetcor analyses of **Ata1** molecule, respectively, were interpreted and the signals of functional groups and atoms in the molecule were analyzed. FTIR spectra of all compounds were taken by ATR method. In the FTIR spectrum of **Ata1**, a broad band belonging to OH stretching vibrations starting from 3300 cm^{-1} and aromatic and aliphatic C-H stretching vibrations in the range of $3055\text{--}2845\text{ cm}^{-1}$ were observed. **Ata1** showed absorption bands at 1723 , 1650 and 1623 cm^{-1} due to CO groups stretching vibrations, respectively. In addition, some absorption bands of this compound were observed in the range of $1607\text{--}1463\text{ cm}^{-1}$ due to C=C stretching vibrations. Also in

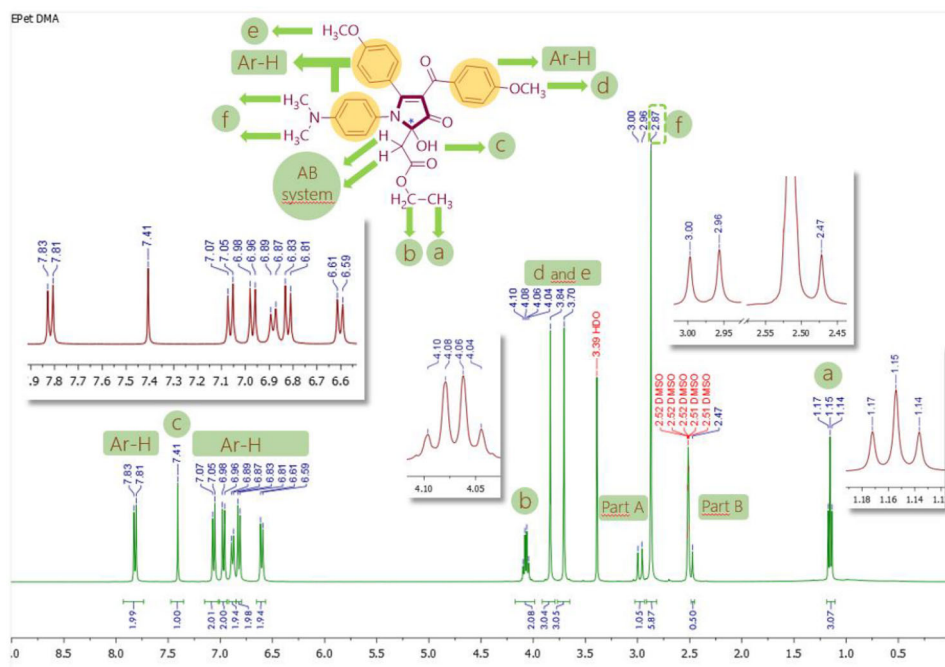


Figure 1. ^1H NMR spectra of compound **Ata1**.

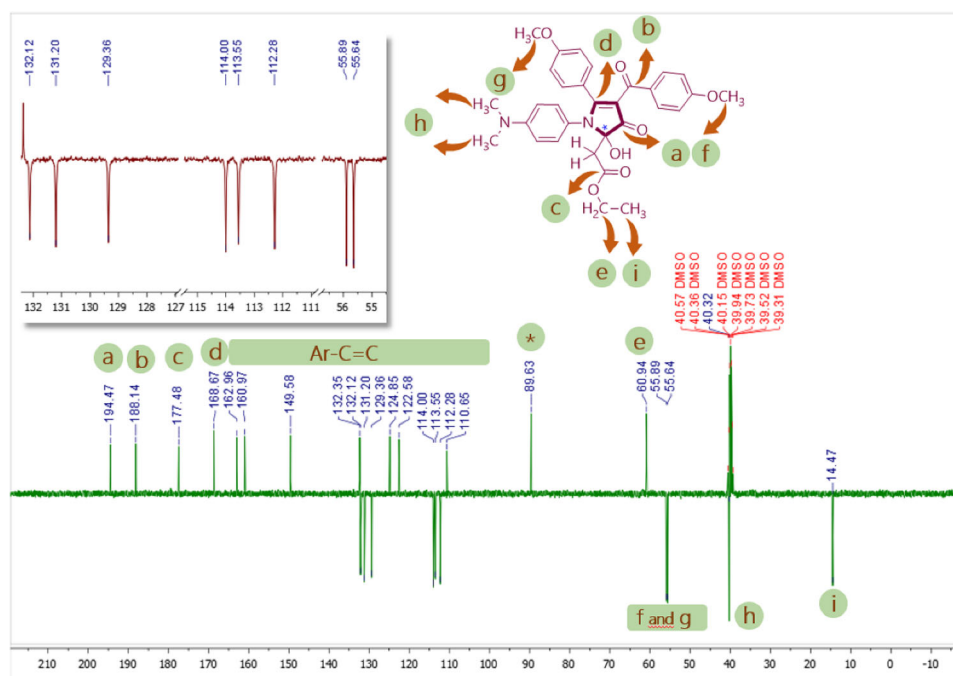


Figure 2. ^{13}C NMR spectra of compound **Ata1**.

this spectrum, there are bands belonging to C-O-C stretching vibrations at 1245 and 1128 cm^{-1} .

Figure 1 shows the ^1H -NMR spectrum of **Ata1** compound dissolved in $\text{DMSO}-d_6$. Accordingly, the multiplet peaks were observed at $\delta = 7.83\text{--}6.59$ ppm belonging to aromatic protons, and the singlet peak was seen at $\delta = 7.41$ ppm due to proton of the OH group. The peaks were observed at 4.07 ppm corresponding to two protons and belonging to methylene protons in the ethoxy group. Peaks belonging to protons in methoxy groups are observed as two singlet peaks at $\delta = 3.84$ and 3.70 ppm. In addition, the AB system

was seen in diastereotopic CH_2 protons adjacent to the asymmetric carbon of pyrrole moiety. The part A of the system consists of the peaks at $\delta = 2.98$ ppm, and the part B of the system is the peaks at $\delta = 2.49$ ppm. Methyl groups in the dimethylamino group were observed as singlets at 2.87 ppm. The triplet signal observed at 1.15 ppm corresponds to three protons and belongs to methyl protons in the ethoxy group.

The ^{13}C -NMR spectrum of **Ata1** compound taken by dissolving $\text{DMSO}-d_6$ is given in Figure 2. Signals of carbonyl groups in this molecule were observed at 194.5 , 188.1 and

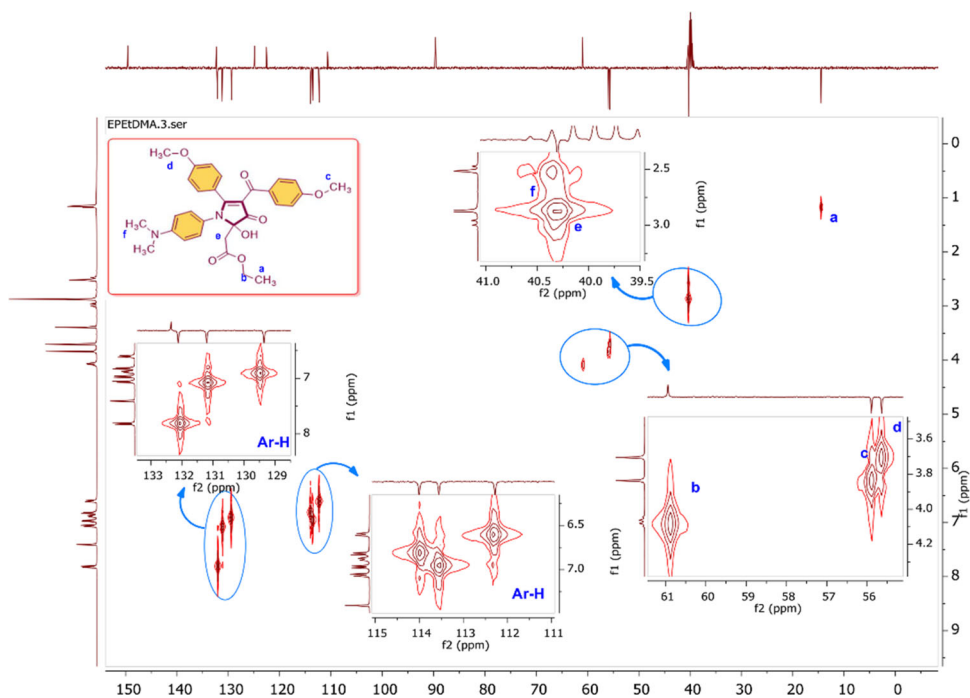


Figure 3. HETCOR spectra of compound **Ata1**.

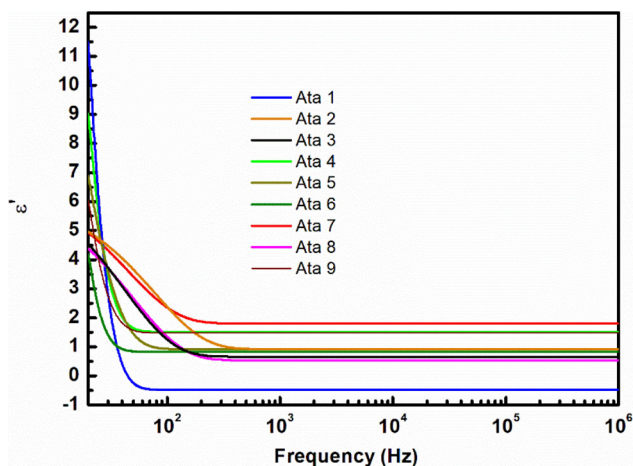


Figure 4. The variation of the real part of permittivity as a function of frequency.

175.5 ppm. The peaks seen between $\delta = 168.7\text{--}110.7$ ppm are the signals of aromatic, aliphatic $\text{C}=\text{C}$ carbon atoms. The signal of the optically active carbon atom was observed at 89.6 ppm. While a signal belonging to the carbon of the OCH_2 group was seen at 60.9 ppm, the signals of the methoxy groups were presented at 55.9 and 55.6 ppm. The signal belonging to the $\text{N}(\text{CH}_3)_2$ group was observed at 40.3 ppm among the solvent signals, while the signal of the CH_2 carbon atom adjacent to the carbonyl group was located under the solvent peaks and was not observed. HETCOR spectrum of **Ata1** that is shown signals in the contour plot with the chemical shifts of proton and carbons that are directly bonded is compatible with ^1H and ^{13}C NMR spectrums (Figure 3). The peaks at 194.5–132.4, 124.8, 122.6, 110.6 and 89.6 ppm are quaternary carbons and are not result in any correlations (this is expected since quaternary carbons do not have protons directly attached ($^1J_{\text{CH}}$)). The

peaks at 132.1–129.4 and 114.0–112.3 ppm are the aromatic carbon signals, which are bonded with the aromatic proton signals present at 7.83–6.59 ppm. The peak (a) at 14.5 ppm is directly bonded to the triplet ($-\text{CH}_3$) at 1.15 ppm. The peak (b) at 60.9 ppm is directly bonded to the quartet ($-\text{CH}_2$) at 4.08 ppm. The peak (c) at 55.9 ppm is directly bonded to the singlet ($-\text{OCH}_3$) at 3.84 ppm. The peak (d) at 55.6 ppm is directly bonded to the singlet ($-\text{OCH}_3$) at 3.70 ppm. The peak (e) at 40.3 ppm is directly bonded to the singlet ($-\text{CH}_2$) at 2.52 ppm. The peak (f) at 40.3 ppm is directly bonded to the singlet ($-\text{N}(\text{CH}_3)_2$) at 2.87 ppm. The ^1H NMR and ^{13}C NMR data of the **Ata1** molecule describe all the carbon and hydrogen atoms in the molecule. Spectroscopic analysis data for the other synthesized compounds confirm the structures of the corresponding compounds (See Supplementary Material).

4.2. Dielectric properties of the samples

Dielectric spectroscopy is a powerful method for any materials for valuable information about polarization behavior, conduction mechanism and dielectric relaxation (Maxwell, 1892). Figure 4 shows the real part of the dielectric constant with increasing angular frequency (ω) plotted in a semi-log scale in the range of 20 Hz–1 MHz for the synthesized samples. When the graph is viewed, a strong decrease appears for the dielectric permittivity values at the low-frequency region that may be explained based on the Maxwell–Wagner model (Kremer & Schönhal, 2002; Maxwell, 1892). In the model, dielectric materials are thought to consist of conducting grains separated by the resistive grain boundaries. After a remarkable decrease, frequency-independent characteristics were observed for all the samples. At 1 kHz frequency, the **Ata7** sample showed a maximum dielectric constant related

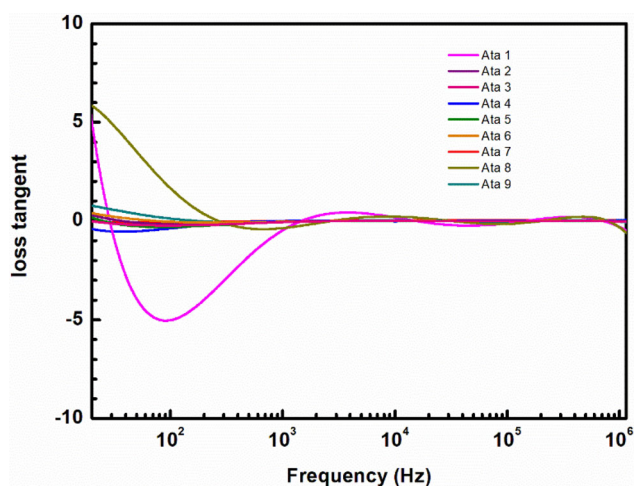


Figure 5. The loss spectrum of the synthesized samples.

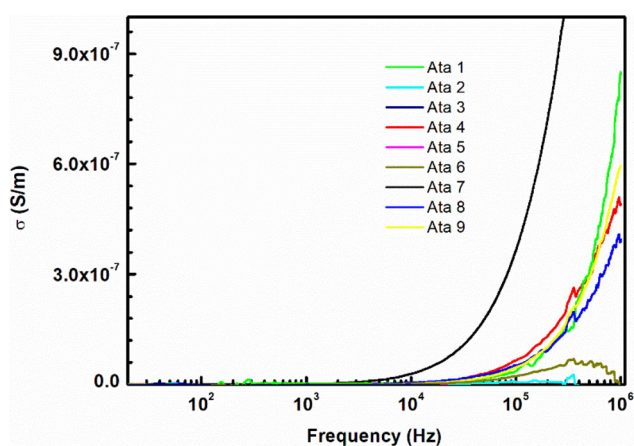


Figure 6. The ac conductivity spectrum of the synthesized samples.

to the measured molecule's polarization. However, in addition to the contribution from molecular polarization, molecular interactions and grain boundaries determine the dielectric constant. The other samples showed similar dielectric characteristics with dielectric constant values close to each other except **Ata1**. **Ata1** sample exhibited negative dielectric values. There are many reasons for the negative capacitance or dielectric permittivity, intentionally or unintentionally doping with small size cations driven by the applied voltage and accumulation at the interface (Wang & Cai, 2012), static electricity of materials (Yan et al., 2013). Alternatively, metamaterials exhibited negative dielectric permittivity values (Li et al., 2009). Negative dielectric permittivity has been observed in the system containing free electrons at the high frequency, but the same achieved at low frequency, even desired frequency for polymer composite material (Ramasamy et al., 2014). This work proved that all of the prepared organic structures were pure and did not contain any cation. We also investigated the probability of metal doping at the moment of pellet pressing procedure from the metal compression chamber after pelleting. The analysis results again exhibited that pressed samples did not contain any metal doping. We tested samples' static electricity that can be reason the observed negative dielectric permittivity. The samples could gain static electricity at the

moment of pressing. We measured the dielectric properties of samples immediately and 15 days after the pressing to explore this suspect. The measurements showed less than 1% deviation from that of the initial measurement. Thus, **Ata1** was considered as a negative dielectric constant material. It has a high electron density, and that may cause the observed negative dielectric constant.

Figure 5 depicts the loss tangent graph of the samples. The loss tangent is given by,

$$\tan \delta = (\epsilon''/\epsilon')$$

where ϵ' and ϵ'' real and imaginary part of permittivity, respectively. According to the graph, **Ata1** and **Ata5** showed maximum dielectric losses at the low frequency. The dielectric losses occur due to the absorption of applied energy, which is generally utilized to rotate dipolar molecules. When the molecular structure of an organic molecule is changed, it produced different loss tangent curves. Thus, while the general shape of the curves is similar, **Ata1** presented different characteristics.

Figure 6 shows the conductivity-frequency graph of all samples. All samples exhibited weak conductivity at low- and middle-frequency regions. With the increasing frequency, an increase in conductivity appears for all samples. Among them, **Ata3** and **Ata1** stand out with their high conductivity response in the high-frequency region. Since the dimethylamino group is electron donating, it donates electrons to the pyrrole ring. For this reason, **Ata3** and **Ata1** conductivity may come to the fore at high frequencies.

4.3. ^1H and ^{13}C NMR chemical shift analyses

The experimental records on the ^{13}C - and ^1H -NMR chemical shifts of the compounds **Ata1-9** dissolved in $\text{DMSO}-d_6$ were used in order to analyze magnetic spectral characterizations of functional groups within their molecular structures. The theoretical NMR results of these nine compounds were obtained by using the GIAO method, B3LYP/6-311++G(d,p) level, IEFPCM solvent model and DMSO solvent within the computational procedure. Some experimental and all computed NMR chemical shift data for carbon and hydrogen atoms within compounds were summarized in Tables S1 and S2.

The carbon atoms were connected by a π bond to the electronegative oxygen atoms within carbonyl groups such as ketone, aldehyde, ester, carboxylic acid and amide resonate in the NMR region between 160 and 220 ppm (Gümüř et al., 2019; Koca et al., 2020). The ketone carbons (labeled as the C5 in all compounds) within ring of 5-atoms were found at 194.0–194.6 ppm (exp.)/197.8–206.3 ppm (calc.), while the other ketone carbons (labeled as the C6, C10, C49) in six compounds (**Ata1**, **Ata2**, **Ata4**, **Ata5**, **Ata7** and **Ata8**) resonated at 188.1–188.4 ppm as experimental and 198.2–199.4 ppm as theoretical. Similarly, the ester carbons (labeled as the C14 in **Ata1** and **Ata2**, the C6 and C14 in **Ata3**, the C29 in **Ata4**, **Ata5** and **Ata7**, the C10 and C25 in **Ata6** and **Ata9** and the C10 in **Ata 8**) in all compounds were obtained at the intervals of 163.0–178.9 ppm and

166.3–185.6 ppm as both experimental and theoretical, respectively. The amide carbons (the C38, C19 and C31 atoms, respectively) within the compounds **Ata7**, **8** and **9** were recorded as resonance peak signals 168.5, 169.1 and 167.4 ppm as experimental and 176.3, 175.9 and 175.6 ppm as computational. The carbons (labeled as the C4 in **Ata1-3** and **8** and the C2 in **Ata4-7** and **9**) within ring of 5-atoms bonded of hydroxy groups in all nine compounds were measured and computed at the intervals of 88.9–89.7 ppm and 97.7–91.7 ppm, respectively. As can be seen in Table S1, the methyl and ethyl carbons within the compounds were measured and computed as resonance signals within upfield region below 61 and 70 ppm, respectively.

The NMR resonance frequency signals for hydroxyl protons (the H43, H42, H37, H40, H39, H34, H43, H24 and H37 atoms, respectively) within all the compounds **Ata1-9** were experimentally recorded at 7.50 ± 0.21 ppm. These values may indicate a weak character O–H...O intramolecular hydrogen bond. The computed NMR values for these hydroxyl protons were obtained at the interval 5.22–6.75 ppm. The protons on the nitrogen atoms of the amide groups the compounds **Ata7**, **8** and **9** were assigned to NMR signals in the region of 7.41–8.00 ppm, while they were computed at values between 5.26 and 6.05 ppm. The experimental and compute NMR chemical shifts for the methyl and ethyl protons within the compounds were found in region below 4.07 and 4.28 ppm, respectively (Table S2).

4.4. UV-Vis. spectroscopic and FMOs analyses

Intramolecular charge transfer properties of the compounds **Ata1-9** were researched by the TD-DFT method at the B3LYP/6-311++G(d,p) computational level. The computed absorption wavelengths and related parameters are listed in Table 2. GaussSum 3.0.1 software (O'boyle et al., 2008) used to obtain the percentages with major contributions of electronic transitions corresponding to the computed wavelengths. The experimental UV spectra of the compounds were recorded in *n,n*-dimethylformamide (DMF) solvent. They were given in Figure S25.

The experimental UV spectra of the compounds contain absorption bands within 264–379-nm region. The UV absorption wavelengths in mentioned this region can correspond to the intra-molecular $\pi \rightarrow \pi^*$ electronic transition, which could result from the presence of conjugated groups in the compounds. The UV wavelengths were computed at the intervals 421.60–325.62 nm for **Ata1**, 422.88–325.35 nm for **Ata2**, 429.95–297.34 nm for **Ata3**, 354.31–325.32 nm for **Ata4**, 354.23–325.70 nm for **Ata5**, 340.66–268.42 nm for **Ata6**, 357.29–326.70 nm for **Ata7**, 349.42–325.72 nm for **Ata8** and 343.88–283.46 nm for **Ata9**. The most likely electronic excitation that can occur within a molecular system is from HOMO to LUMO because the energy difference between HOMO and LUMO is less compared with other molecular orbital transitions. In our study, the possible HOMO→LUMO electronic transitions for the compounds **Ata1-9** were computed at 421.60/0.0936/97% for **Ata1**, 422.88/0.0975/97% for **Ata2**, 429.95/0.0659/99% for **Ata3**, 354.31/0.1812/53% and

343.05/0.2834/36% for **Ata4**, 354.23/0.1867/54% and 342.88/0.2756/35% for **Ata5**, 340.66/0.0464/19% and 329.67/0.3565/79% for **Ata6**, 357.29/0.2105/52% and 345.25/0.3508/41% for **Ata7**, 349.42/0.3150/57% and 333.82/0.1562/24% for **Ata8** and 343.88/0.0767/30% and 334.35/0.3172/68% for **Ata9** with values of wavelength/oscillator strength/percentage contribution. As can be seen from charge localizations on HOMO and LUMO in Figure S26, they were mainly formed as bonding pi and anti-bonding pi molecular orbital styles of aromatic groups, respectively. These HOMO→LUMO electronic transitions can be interpreted as $\pi \rightarrow \pi^*$ character.

LUMO (lowest unoccupied molecular orbital) and HOMO (highest occupied molecular orbital) that are known as FMOs play an important role in determining intramolecular electronic transitions and many molecular electronic features in a molecular (Fukui, 1982; Geerlings et al., 2003; Parr & Pearson, 1983; Pearson, 1986; Zhan et al., 2003). Some global reactivity parameters defined in Table 3 were computed depending on LUMO and HOMO energy values of the compounds **Ata1-9**. E_{LUMO} , E_{HOMO} and $|E_{HOMO} - E_{LUMO}|$ values were obtained as –2.045, –5.556 and 3.510 eV for **Ata1**, –2.053, –5.553 and 3.500 eV for **Ata2**, –2.113, –5.575 and 3.462 eV for **Ata3**, –2.231, –6.411 and 4.180 eV for **Ata4**, –2.238, –6.417 and 4.179 eV for **Ata5**, –2.173, –6.505 and 4.332 eV for **Ata6**, –2.315, –6.353 and 4.038 eV for **Ata7**, –2.268, –6.450 and 4.182 eV for **Ata8** and –2.278, –6.528 and 4.250 eV for **Ata9**. The order within the energy band gaps $|E_{HOMO} - E_{LUMO}|$ of the compounds is **Ata3**<**Ata2**<**Ata1**<**Ata7** <**Ata5**<**Ata4** <**Ata8**<**Ata9**<**Ata6**. It is well known that the smaller the energy band gap of molecules, the more easily molecule can be excited, or vice versa. Moreover, according to low or large values of energy band gap, molecule is called as chemically soft or hard. According to this, the compound **Ata3** is softer and easier excitable than others. Likewise, the orders within LUMOs and HOMOs of the compounds are **Ata7**<**Ata9**<**Ata8**<**Ata5**<**Ata4**<**Ata6**<**Ata3**<**Ata2**<**Ata1** and **Ata9**<**Ata6**<**Ata8**<**Ata5**<**Ata4**<**Ata7** <**Ata3**<**Ata1** <**Ata2**, respectively. According to these results computed of LUMO and HOMO, the highest ionization potential ($I = -E_{HOMO}$) and electron affinity ($A = -E_{LUMO}$) values are for the compounds **Ata9** and **Ata7**, whereas their lowest values belong to the compounds **Ata2** and **Ata1**, respectively. The chemical potentials ($\mu = -(I + A)/2$) for the compounds were computed as –3.801 eV for **Ata1**, –3.803 eV for **Ata2**, –3.844 eV for **Ata3**, –4.321 eV for **Ata4**, –4.328 eV for **Ata5**, –4.339 eV for **Ata6**, –4.334 eV for **Ata7**, –4.359 eV for **Ata8** and –4.403 eV for **Ata9**.

4.5. Nonlinear optical properties

The optical properties of matter can be expressed as the reaction of the electrons within it to an electric field. As it is known, the electric field vector of the light sent on the matter polarizes it. The polarity of an atom or molecule is a measure of how easily nuclei and electrons can move from equilibrium states and it is an electrical characteristic of matter. The design of molecules with nonlinear optical (NLO) properties is a current research topic in modern

Table 2. The computed UV spectral parameters of the compounds.

Ata1			
$\lambda_{\text{calc.}}$ (nm)	f	ΔE (eV)	Computed major transitions in MOs
421.60	0.0936	2.9408	H \rightarrow L(97%)
370.93	0.0481	3.3425	H \rightarrow L + 1(93%)
337.85	0.1252	3.6698	H-1 \rightarrow L(42%), H-4 \rightarrow L(31%), H-1 \rightarrow L + 1(10%)
333.33	0.1387	3.7196	H-4 \rightarrow L(49%), H-1 \rightarrow L(22%), H-4 \rightarrow L + 1(11%)
325.62	0.2041	3.8076	H-4 \rightarrow L + 1(39%), H-1 \rightarrow L(31%), H-2 \rightarrow L(12%)
Ata2			
$\lambda_{\text{calc.}}$ (nm)	f	ΔE (eV)	Computed major transitions in MOs
422.88	0.0975	2.9319	H \rightarrow (97%)
372.35	0.0488	3.3298	H \rightarrow L + 1(93%)
338.50	0.1343	3.6627	H-1 \rightarrow L(46%), H-4 \rightarrow L(28%), H-1 \rightarrow L + 1(11%)
333.26	0.1137	3.7203	H-4 \rightarrow L(48%), H-1 \rightarrow L(14%), H-4 \rightarrow L + 1(12%), H-4 \rightarrow L(11%)
325.35	0.2021	3.8108	H-4 \rightarrow L + 1(35%), H-1 \rightarrow L(34%)
Ata3			
$\lambda_{\text{calc.}}$ (nm)	f	ΔE (eV)	Computed major transitions in MOs
429.95	0.0659	2.8837	H \rightarrow (99%)
332.73	0.1232	3.7263	H-3 \rightarrow L(52%), H-1 \rightarrow L(41%)
323.60	0.2732	3.8314	H-1 \rightarrow L(57%), H-3 \rightarrow L(38%)
303.74	0.1234	4.0820	H-4 \rightarrow L(93%)
297.34	0.0590	4.1698	H \rightarrow L + 1(84%), H \rightarrow L + 3(12%)
Ata4			
$\lambda_{\text{calc.}}$ (nm)	f	ΔE (eV)	Computed major transitions in MOs
354.31	0.1812	3.4993	H \rightarrow (53%), H-3 \rightarrow L(35%)
343.05	0.2834	3.6142	H-3 \rightarrow L(50%), H \rightarrow (36%)
338.76	0.1242	3.6599	H-4 \rightarrow L(64%), H-4 \rightarrow L + 1(18%)
329.28	0.0696	3.7653	H-1 \rightarrow L(51%), H \rightarrow L + 1(15%), H-4 \rightarrow L + 1(10%)
325.32	0.0309	3.8112	H-1 \rightarrow L(42%), H \rightarrow L + 1(20%), H-4 \rightarrow L(16%), H-4 \rightarrow L + 1(11%)
Ata5			
$\lambda_{\text{calc.}}$ (nm)	f	ΔE (eV)	Computed major transitions in MOs
354.23	0.1867	3.5001	H \rightarrow (54%), H-3 \rightarrow L(34%)
342.88	0.2756	3.6160	H-3 \rightarrow L(51%), H \rightarrow (35%)
339.04	0.1309	3.6569	H-4 \rightarrow L(68%), H-4 \rightarrow L + 1(16%)
329.75	0.0699	3.7599	H-1 \rightarrow L(56%), H \rightarrow L + 1(13%)
325.70	0.0273	3.8067	H-1 \rightarrow L(37%), H \rightarrow L + 1(23%), H-4 \rightarrow L(14%), H-4 \rightarrow L + 1(13%)
Ata6			
$\lambda_{\text{calc.}}$ (nm)	f	ΔE (eV)	Computed major transitions in MOs
340.66	0.0464	3.6395	H-4 \rightarrow L(69%), H \rightarrow (19%)
329.67	0.3565	3.7609	H \rightarrow (79%), H-4 \rightarrow L(14%)
325.09	0.1508	3.8139	H-1 \rightarrow L(87%)
276.30	0.0072	4.4873	H-3 \rightarrow L(76%)
268.42	0.0079	4.6191	H-4 \rightarrow L(89%)
Ata7			
$\lambda_{\text{calc.}}$ (nm)	f	ΔE (eV)	Computed major transitions in MOs
357.29	0.2105	3.4701	H \rightarrow (52%), H-3 \rightarrow L(33%)
345.25	0.3508	3.5911	H \rightarrow (41%), H-3 \rightarrow L(38%)
341.25	0.0920	3.6332	H-4 \rightarrow L(61%), H-4 \rightarrow L + 1(15%), H-3 \rightarrow L(10%)
333.54	0.1139	3.7172	H-1 \rightarrow L(80%)
326.70	0.0085	3.7951	H \rightarrow L + 1(26%), H-4 \rightarrow L + 1(22%), H-2 \rightarrow L + 1(16%), H-4 \rightarrow L(15%), H-1 \rightarrow L(11%)
Ata8			
$\lambda_{\text{calc.}}$ (nm)	f	ΔE (eV)	Computed major transitions in MOs
349.42	0.3150	3.5483	H \rightarrow (57%), H-3 \rightarrow L(20%)
343.37	0.1132	3.6108	H-3 \rightarrow L(27%), H-4 \rightarrow L(26%), H \rightarrow (14%)
333.82	0.1562	3.7141	H \rightarrow (24%), H \rightarrow L + 1(16%), H-3 \rightarrow L(16%), H-4 \rightarrow L + 1(15%), H-1 \rightarrow L(10%)
329.96	0.1459	3.7575	H-4 \rightarrow L(58%), H-1 \rightarrow L(20%), H-3 \rightarrow L(14%)
325.72	0.1232	3.8065	H-1 \rightarrow L(57%), H \rightarrow L + 1(14%)
Ata9			
$\lambda_{\text{calc.}}$ (nm)	f	ΔE (eV)	Computed major transitions in MOs
343.88	0.0767	3.6055	H-4 \rightarrow L(58%), H \rightarrow (30%)
334.35	0.3172	3.7082	H \rightarrow (68%), H-4 \rightarrow L(27%)
330.05	0.2328	3.7565	H-1 \rightarrow L(94%)
291.73	0.0267	4.2500	H \rightarrow L + 1(88%)
283.46	0.1092	4.3740	H-1 \rightarrow L + 1(86%)

$\lambda_{\text{calc.}}$: computed wavelength, f: oscillator strength, ΔE : excitation energy, MO: molecular orbital.

communication technology and optical data storage. Bipolar molecules with acceptor–donor groups are the most researched NLO materials. NLO materials are categorized as semiconductor layered structures. Therefore, many types of inorganic, organic and organometallic molecular systems are being studied for NLO activity. The nonlinear optical

properties of the molecules arise from the delocalized π -electrons moving through the molecule. Increasing conjugation in the molecule leads to an increase in nonlinear optical properties. When we look at the literature (Hinchliffe & Soscún M, 1994), we notice that there is a reciprocal relationship between the polarizability of molecules and the HOMO-

Table 3. HOMOs and LUMOs energy values and other related parameters computed in DMSO solvent of the title compounds.

Parameters (eV)	Ata1	Ata2	Ata3	Ata4	Ata5	Ata6	Ata7	Ata8	Ata9
E_{LUMO}	-2.045	-2.053	-2.113	-2.231	-2.238	-2.173	-2.315	-2.268	-2.278
E_{HOMO}	-5.556	-5.553	-5.575	-6.411	-6.417	-6.505	-6.353	-6.450	-6.528
Energy band gap	3.510	3.500	3.462	4.180	4.179	4.332	4.038	4.182	4.250
Ionization potential	5.556	5.553	5.575	6.411	6.417	6.505	6.353	6.450	6.528
Electron affinity	2.045	2.053	2.113	2.231	2.238	2.173	2.315	2.268	2.278
Chemical hardness	1.755	1.750	1.731	2.090	2.089	2.166	2.019	2.091	2.125
Chemical softness	0.285	0.286	0.289	0.239	0.239	0.231	0.248	0.239	0.235
Electronegativity	3.801	3.803	3.844	4.321	4.328	4.339	4.334	4.359	4.403
Chemical potential	-3.801	-3.803	-3.844	-4.321	-4.328	-4.339	-4.334	-4.359	-4.403
Electrophilicity index	4.115	4.132	4.268	4.466	4.482	4.347	4.653	4.542	4.561
Maximum charge transfer index	2.165	2.173	2.221	2.067	2.071	2.004	2.147	2.084	2.072

LUMO energy range. The smaller the HOMO-LUMO energy difference of the molecule, the easier the electron distribution can be directed and the greater the polarization. Therefore, it will not be surprising that β is large in a molecule with a small HOMO-LUMO energy range and such a molecule can be considered as a material with nonlinear optical properties. However, it should be noted that the HOMO-LUMO energy range is not a sufficient predictor for the β value of the molecule. Another way to increase the nonlinear optical properties of a molecule is to add donor and acceptor groups to the molecule. If the delocalization of the π electron cloud on the molecule increases, the polarizability value of the molecules increases (Verbiest et al., 1997; Wolff & Wortmann, 1999). Theoretical and experimental studies show that the first- and second-order hyper-polarizability of molecules is significantly affected by the environment.

In this section as theoretically, the mean polarizability (α_{total}) and its components, the anisotropy of polarizability ($\Delta\alpha$), the first-order hyper-polarizability (β_0) and its components and the dipole moments (μ_x , μ_y , μ_z) of **Ata1-9** molecules were computed with B3LYP model and 6-311++G(d,p) basis set. For reference NLO material urea molecule, these parameters (α_{total} , $\Delta\alpha$ and β_0) was reported as $5.07643717 \times 10^{-24}$ esu, $2.13568262 \times 10^{-24}$ esu and $7.2228469891 \times 10^{-31}$ esu, respectively and the urea molecule is a pretty good reference for organic materials. For our computations, the used equations are follows:

$$\alpha_{\text{total}} = \frac{1}{3}(\alpha_{xx} + \alpha_{yy} + \alpha_{zz}) \quad (1)$$

$$\Delta\alpha = \frac{1}{\sqrt{2}} \left[(\alpha_{xx} - \alpha_{yy})^2 + (\alpha_{yy} - \alpha_{zz})^2 + (\alpha_{zz} - \alpha_{xx})^2 + 6\alpha_{xz}^2 + 6\alpha_{xy}^2 + 6\alpha_{yz}^2 \right]^{1/2} \quad (2)$$

$$\beta_0 = \left[(\beta_{xxx} + \beta_{yyy} + \beta_{zzz})^2 + (\beta_{yyy} + \beta_{zzz} + \beta_{yxx})^2 + (\beta_{zzz} + \beta_{zzx} + \beta_{zyy})^2 \right]^{1/2} \quad (3)$$

$$\mu_{\text{total}} = (\mu_x^2 + \mu_y^2 + \mu_z^2)^{1/2} \quad (4)$$

The obtained NLO values of **Ata1-9** molecules were presented in Table S3; additionally, their comparison with urea molecule was given in Table S4. From Table S3 and S4, we can say that the order of the dipole moment magnitudes is as follows: **Ata3** $\mu_{\text{total}} >$ **Ata2** $\mu_{\text{total}} >$ **Ata1** $\mu_{\text{total}} >$ **Ata6** $\mu_{\text{total}} >$ **Ata5** $\mu_{\text{total}} >$ **Ata4** $\mu_{\text{total}} >$ **Ata8** $\mu_{\text{total}} >$ **Ata9** $\mu_{\text{total}} >$ **Ata7** μ_{total} . The groups donating electrons to the pyrrole ring increase the electron density in the ring, which increases the dipole moment in the ring. In the order of **Ata3** $>$ **Ata2** $>$ **Ata1**, the ester group in the fourth position

of the **Ata3** compound is more easily polarized than the aromatic ring, so it is expected that the order will come out in this way. Secondly, the order of the first-order hyper-polarizabilities (β_0) was obtained as follows: **Ata8** $\beta_0 >$ **Ata7** $\beta_0 >$ **Ata3** $\beta_0 >$ **Ata9** $\beta_0 >$ **Ata5** $\beta_0 >$ **Ata4** $\beta_0 >$ **Ata2** $\beta_0 >$ **Ata6** $\beta_0 >$ **Ata1** β_0 . In light of the literature information given above, it is expected for a molecule with a small HOMO-LUMO energy range to have higher β . But in our molecular system, the β value of the **Ata8** molecule is greater than the others. The expected result is **Ata3** according to the literature (Verbiest et al., 1997; Wolff & Wortmann, 1999). As a consequence the β values of pyrroles containing amide group were found to be high. However, it should be noted that the HOMO-LUMO energy range is not a sufficient predictor for the β value of the molecule. In other words, increasing the ground state charge asymmetry of the molecule by attaching acceptor and donor groups to the ends of the molecule will increase the first-order hyper-polarity value. As the third, the order of the mean polarizability (α_{total}) is **Ata1** $\alpha_{\text{total}} >$ **Ata7** $\alpha_{\text{total}} >$ **Ata2** $\alpha_{\text{total}} >$ **Ata8** $\alpha_{\text{total}} >$ **Ata4** $\alpha_{\text{total}} >$ **Ata5** $\alpha_{\text{total}} >$ **Ata3** $\alpha_{\text{total}} >$ **Ata9** $\alpha_{\text{total}} >$ **Ata6** α_{total} . Finally, the order of anisotropy of polarizability ($\Delta\alpha$) was found as follows: **Ata7** $\Delta\alpha >$ **Ata1** $\Delta\alpha >$ **Ata8** $\Delta\alpha >$ **Ata4** $\Delta\alpha >$ **Ata5** $\Delta\alpha >$ **Ata2** $\Delta\alpha >$ **Ata9** $\Delta\alpha >$ **Ata3** $\Delta\alpha >$ **Ata6** $\Delta\alpha$.

4.6. Molecular electrostatic potential

Molecular electrostatic potential (MEP) analysis is a useful method that shows the charge distributions of molecular systems, including biomolecules and drugs, in three dimensions and is often used to determine chemical reactivities, hydrogen bond interactions, electrophilic and nucleophilic regions (Luque et al., 2000; Scrocco & Tomasi, 1973). MEP analysis is very important in showing molecular size, shape and positive, negative, neutral electrostatic potential regions simultaneously and in investigating the relationship between physicochemical property and molecular structure. In addition, MEP is related to the molecule's dipole moment, electronegativity, partial charges and chemical reactivity region. It provides a visual method for understanding the relative polarity of a molecule. The positive electrostatic potential corresponds to the repulsion of the proton by the atomic nucleus in regions of low electron density, while the negative electrostatic potential corresponds to the attraction of the proton by the concentrated electron density of the

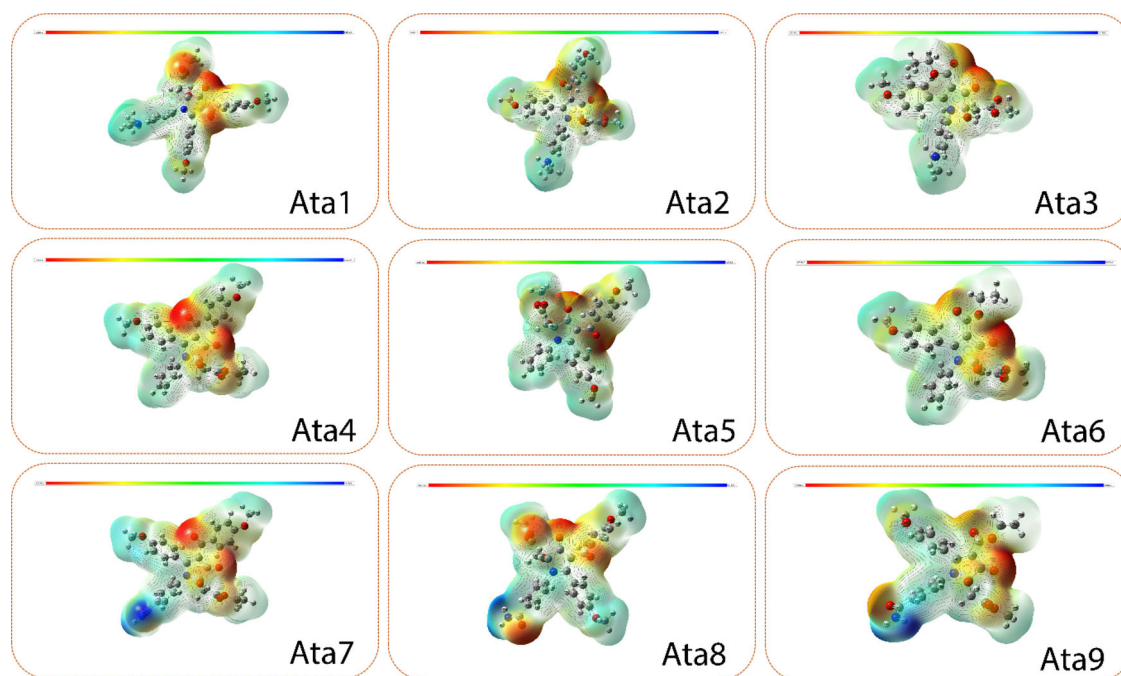


Figure 7. The MEP analysis of the **Ata1-9** compounds at B3LYP/6-311++G(d,p) level.

molecule. The different electrostatic potential values on the MEP surface are represented by different colors: Red, blue and green are the most negative, most positive and zero electrostatic potential regions, respectively. Identifying these regions means determining intramolecular and intermolecular interaction regions. Increases in potential are identified in the order of red < orange < yellow < green < blue. The value of the electrostatic potential is largely responsible for the binding of a substrate to the receptor binding sites because the receptor and the corresponding ligands recognize each other at the molecular surfaces.

In this section, the MEP surfaces of **Ata1-9** were calculated by DFT-B3LYP/6-311 + G(d,p) level over the optimized structures by using *.chk files and their MEP surfaces and potential scales are shown in [Figure 7](#). The potential color scales of **Ata1-9** molecules were calculated in the range between $-6.596e-2$ and $6.596e-2$ for **Ata1**; in the range between $-6.486e-2$ and $6.486e-2$ for **Ata2**, in the range between $-8.815e-2$ and $8.815e-2$ for **Ata3**, in the range between $-6.327e-2$ and $6.327e-2$ for **Ata4**, in the range between $-6.306e-2$ and 6.306 for **Ata5**, in the range between $-6.328e-2$ and $6.328e-2$ for **Ata6**, in the range between $-6.045e-2$ and $6.045e-2$ for **Ata7**, in the range between $-5.814e-2$ and $5.814e-2$ for **Ata8** and in the range between $-5.986e-2$ and $5.986e-2$ for **Ata9** molecule. For **Ata1**, **Ata2** and **Ata3** molecules, it can be clearly seen that the negative region is mainly localized over the O13, O8, O15 atoms; for **Ata4**, **Ata5** and **Ata6** molecules, it can be clearly seen that the negative region is mainly localized over the O11 and O9 atom; for **Ata7** molecule, it can be clearly seen that the negative region is mainly focused on the O11, O9 and O39 atom; for **Ata8** molecule, it can be clearly seen that the negative region is mainly focused on the O6, O50, O11 and O20 atoms; and for **Ata9** molecule, it can be clearly seen that the negative region is mainly

focused on the O9, O32 and O11 atoms, which are the most reactive parts of the molecules. On the other hand, the positive regions are focused over hydrogen atoms (with normal blue distribution) for **Ata1**, **Ata2**, **Ata3**, **Ata4**, **Ata5** and **Ata6** molecules; additionally for **Ata7**, **Ata8** and **Ata9** molecules, dark blue points (positive regions) were focused on H67-H68, H32-H33 and H54-H55 molecules, respectively. These points indicate a possible nucleophilic attack site. As a result, we can say that the positive and negative regions provide information about the region where the compound can have intermolecular interactions.

4.7. Molecular docking study

Molecular docking plays a leading role in drug design, and many docking programs are used for these theoretical studies. The docking process is a program that examines the interactions and movements between ligand and protein during binding. For the docking, ligands and proteins with a known three-dimensional structure are needed. In this part, the molecular docking studies of **Ata1-9** ligands were investigated by the AutoDock Vina program (Trott & Olson, 2010). Primarily, the receptors or targets were determined with biological activity program-PASS website (Filimonov et al., 2014; Filimonov et al., 2014), and Pass analysis results for Pa > Pi of the title ligands are given [Table 4](#). According to PASS online results, our title molecules have two important activity as CYP2H substrate (PDB: 3TDA) and antieczematic (PDB: 3RZE) activity. PDB structures for CYP2H substrate and antieczematic were downloaded from RCSB (Protein Data Bank) (Berman et al., 2003) according to the determined activities. Later, on two proteins heteroatoms involving the ligands, ions and water molecules were removed and polar hydrogen atoms were added. The optimized geometries of **Ata1-9** molecules were used for PDB format as ligand. In this step, all

Table 4. Pass analysis results for Pa > Pi of the title compounds.

Ata1			Ata2			Ata3		
Pa	Pi	Activity	Pa	Pi	Activity	Pa	Pi	Activity
0.800	0.017	CYP2H substrate	0.835	0.012	CYP2H substrate	0.877	0.008	CYP2H substrate
0.782	0.022	Antieczemetic	0.690	0.049	Antieczemetic	0.754	0.029	Antieczemetic
0.483	0.018	Antibacterial	0.496	0.017	Antibacterial	0.554	0.024	Analeptic
0.418	0.028	H ⁺ -exporting ATPase inhibitor	0.422	0.034	P-glycoprotein substrate	0.550	0.049	CYP3A2 substrate
0.413	0.037	P-glycoprotein substrate	0.448	0.077	HIF1A expression inhibitor	0.485	0.018	Antibacterial
0.431	0.062	Antiviral (Rhinovirus)	0.406	0.045	Antimetastatic	0.520	0.055	CYP3A substrate
Ata4			Ata5			Ata6		
Pa	Pi	Activity	Pa	Pi	Activity	Pa	Pi	Activity
0.837	0.012	Antieczemetic	0.777	0.024	Antieczemetic	0.827	0.013	CYP2H substrate
0.666	0.045	CYP2H substrate	0.731	0.029	CYP2H substrate	0.817	0.015	Antieczemetic
0.558	0.071	Phosphatase inhibitor	0.542	0.045	HIF1A expression inhibitor	0.590	0.020	Analeptic
0.529	0.057	Acetylcholine neuromuscular blocking agent	0.560	0.069	Phosphatase inhibitor	0.533	0.019	Histamine release stimulant
0.489	0.034	Histamine release stimulant	0.500	0.036	Antinociceptive	0.550	0.049	CYP3A2 substrate
0.477	0.034	Antiviral (Rhinovirus)	0.589	0.130	Gluconate 2-dehydrogenase (acceptor) inhibitor	0.553	0.073	Phosphatase inhibitor
Ata7			Ata8			Ata9		
Pa	Pi	Activity	Pa	Pi	Activity	Pa	Pi	Activity
0.783	0.022	Antieczemetic	0.693	0.048	Antieczemetic	0.770	0.022	CYP2H substrate
0.581	0.077	CYP2H substrate	0.650	0.050	CYP2H substrate	0.767	0.026	Antieczemetic
0.433	0.024	Antibacterial	0.449	0.022	Antibacterial	0.593	0.079	Nootropic
0.507	0.104	Phosphatase inhibitor	0.504	0.106	Phosphatase inhibitor	0.510	0.030	Analeptic
0.423	0.040	Antimetastatic	0.433	0.037	Antimetastatic	0.521	0.094	Phosphatase inhibitor
0.434	0.060	Antiviral (Rhinovirus)	0.464	0.070	HIF1A expression inhibitor	0.430	0.024	Antibacterial

preparations for both ligands and targets were made by with Discover Studio Visualizer 4.0 (DSV 4.0) software (<http://www.3dsbiovia.com/>). Active residues of target proteins were determined as follows: For 3RZE active residues are ARG1145, ASN1144, PRO1143, THR1142, ARG1080, ARG1076, ASN1055, ASN1053, ARG1014, GLU1011, TYR458, HIS450, PHE435, PHE432, TYR431, TRP428, ASN198, LYS191, LYS179, ASP178, TRP158, ILE115, THR112, SER111, TYR108 and ASP107; for 3TDA (A chain) active residues are PHE483, GLY445, LEU444, CYS443, ARG441, SER437, PHE436, PRO435, ASP422, LEU399, HIS376, VAL374, GLN364, THR313, THR309, ALA305, SER304, LEU302, ASP301, ALA300, GLU287, GLU273, ASP270, HIS258, HIS246, GLN244, GLU216, ARG132, TRP128, PHE120 and ARG101. Therefore, the grid parameters were also determined considering these active residues as follows: 112 × 92 × 102 Å³ *x,y,z* dimensions, 0.375 Å space and 15.751, 33.517, 26.546 *x,y,z* centers for **Ata1-9** + 3RZE; 126 × 114 × 116 Å³ *x,y,z* dimensions, 0.375 Å space and 5.282, 23.83, 3.291 *x,y,z* centers for **Ata1-9** + 3TDA (A chain). As to be in molecular docking studies in the literature (de Lima et al., 2017; Ea de Lima et al., 2016; Kuca et al., 2018), via help of AutoDock Vina program, the molecular docking result outputs computed for 10 different conformational poses of the ligand compounds **Ata 1-9** docked into the target receptor macromolecules (3RZE and 3TDA) are listed in Tables 5 and 6, respectively. For molecular docking analysis, the starting ground state molecular conformational forms of the ligand compounds were obtained by using DFT-B3LYP/6-311++G(d,p) computational level of theoretical model. The comments on the interaction results were performed for the best conformational poses with the lowest interacting energies obtained of the ligand compounds docked into the target macromolecules 3RZE and 3TDA. Additionally, in these tables inhibition constants and the number of hydrogen bonding were given in the bottom lines. Here, the inhibition constants for docking interactions were computed by $K_i = \exp(\Delta G/RT)$ equation (ΔG , R and T are the docking

binding energy, gas constant (1.9872036×10^{-3} kcal/mol) and room temperature (298.15 K), respectively).

According to the affinity binding energies, the best bindings were determined between **Ata7** and **Ata8** compounds and antieczemetic/3RZE protein with same -7.4 kcal/mol energy, $3.76496 \mu\text{M}$ inhibition constant and six hydrogen bonding for **Ata7** and four hydrogen bonding for **Ata8** as shown in Table 5. Additionally, molecular docking results as 3D (a) and 2D (b) forms are shown in Figure 8 (**Ata7**-3RZE interactions).

Finally, the respective docking parameters such as binding energy value, number of hydrogen bonds and inhibition constants involved in bonding against receptor CYP2H substrate/3TDA (A chain) are reported in Table 6. *In silico* molecular docking from Table 6, results reveal that **Ata1** molecule under investigation exhibit excellent binding energy -8.1 kcal/mol containing one hydrogen bond with amino acid residue THR54 of CYP2H substrate/3TDA (A chain) and its inhibition constant is $1.1552 \mu\text{M}$. On the other hand, the most hydrogen bonds (the number of hydrogen bondings) were seen in the interaction between **Ata9** ligand and CYP2H substrate/3TDA (A chain) receptor and its inhibition constant is $12.2706 \mu\text{M}$. Additionally, molecular docking results as 3D (a) and 2D (b) shapes are shown in Figure 9 (**Ata1**-3TDA (A chain) interactions).

Although we cannot say the statement precisely because we do not have experimental data, these results concluded that the compounds are potent inhibitor for antieczemetic/3RZE and CYP2H substrate/3TDA (A chain).

4.8. Drug-likeness and physicochemical properties

Drug-likeness and physicochemical properties are very important in drug design. The pharmacokinetic parameters were first put forward in theory in 1997 when Lipinski et al. published five rules based on the investigation of the

Table 5. AutoDock Vina results of the binding affinity and RMSD values of different poses in Antieczematic/3RZE protein inhibitor of the title compounds.

Mode	Ata1-3RZE			Ata2-3RZE			Ata3-3RZE		
	affinity (kcal/mol)	rmsd l.b.	rmsd u.b.	affinity (kcal/mol)	rmsd l.b.	rmsd u.b.	affinity (kcal/mol)	rmsd l.b.	rmsd u.b.
1	-6.9	0.000	0.000	-6.9	0.000	0.000	-6.4	0.000	0.000
2	-6.4	36.374	39.990	-6.7	16.807	21.233	-6.3	1.858	6.353
3	-6.4	18.169	21.565	-6.2	14.929	17.776	-6.2	2.084	6.128
4	-6.1	36.589	40.193	-6.2	2.016	2.756	-5.7	18.424	22.204
5	-6.0	16.841	19.948	-6.1	3.165	5.061	-5.5	46.390	49.031
6	-5.8	19.423	22.228	-6.0	19.245	22.188	-5.3	22.672	26.335
7	-5.8	20.537	23.928	-6.0	26.785	32.037	-5.3	20.912	23.580
8	-5.7	18.705	22.482	-6.0	46.768	49.553	-5.2	3.105	7.210
9	-5.7	19.457	21.976	-6.0	25.958	31.127	-5.2	42.483	43.863
10	-5.7	12.575	16.901	-5.9	15.809	20.009	-5.2	43.627	46.792
Inhibition constant:8.75514 μM			Inhibition constant:5.27669 μM			Inhibition constant:20.3594 μM			
Number of hydrogen bonding: 4			Number of hydrogen bonding: 2			Number of hydrogen bonding: 5			
Mode	Ata4-3RZE			Ata5-3RZE			Ata6-3RZE		
	affinity (kcal/mol)	rmsd l.b.	rmsd u.b.	affinity (kcal/mol)	rmsd l.b.	rmsd u.b.	affinity (kcal/mol)	rmsd l.b.	rmsd u.b.
1	-7.2	0.000	0.000	-7.2	0.000	0.000	-6.1	0.000	0.000
2	-6.5	2.330	4.982	-6.4	2.507	6.012	-5.9	40.909	43.869
3	-6.3	2.357	6.778	-6.3	36.319	39.356	-5.8	18.080	20.476
4	-6.3	2.107	6.055	-6.2	16.637	20.868	-5.8	18.260	21.015
5	-6.0	14.105	17.368	-6.1	2.425	8.263	-5.7	40.747	43.888
6	-6.0	15.588	20.016	-6.1	36.945	39.957	-5.7	41.058	44.207
7	-5.9	17.721	20.237	-6.0	33.829	37.092	-5.6	18.511	20.999
8	-5.7	39.910	43.071	-5.9	18.059	20.695	-5.5	2.726	3.690
9	-5.7	19.769	21.879	-5.9	3.117	8.597	-5.5	18.571	20.723
10	-5.7	40.409	43.426	-5.9	15.342	20.033	-5.4	29.984	34.841
Inhibition constant:5.27669 μM			Inhibition constant:5.27669 μM			Inhibition constant:33.7806 μM			
Number of hydrogen bonding: 2			Number of hydrogen bonding: 2			Number of hydrogen bonding: 0			
Mode	Ata7-3RZE			Ata8-3RZE			Ata9-3RZE		
	affinity (kcal/mol)	rmsd l.b.	rmsd u.b.	affinity (kcal/mol)	rmsd l.b.	rmsd u.b.	affinity (kcal/mol)	rmsd l.b.	rmsd u.b.
1	-7.4	0.000	0.000	-7.4	0.000	0.000	-6.6	0.000	0.000
2	-6.6	15.301	17.588	-7.2	2.225	6.816	-6.5	2.293	5.341
3	-6.6	4.830	8.366	-6.8	1.880	5.546	-5.8	17.479	20.873
4	-6.6	35.333	39.715	-6.6	12.882	17.421	-5.7	37.023	39.869
5	-6.5	2.710	7.471	-6.5	36.330	40.259	-5.7	28.736	31.893
6	-6.4	36.606	40.887	-6.3	3.004	7.008	-5.6	25.759	29.448
7	-6.4	36.373	40.944	-6.2	26.600	32.019	-5.5	42.950	46.022
8	-6.3	16.188	19.004	-6.2	2.825	7.504	-5.5	17.664	21.097
9	-6.3	16.800	22.022	-6.1	46.690	49.446	-5.5	22.902	26.062
10	-6.0	27.869	31.770	-6.1	2.749	7.242	-5.5	20.032	22.936
Inhibition constant:3.76496 μM			Inhibition constant:3.76496 μM			Inhibition constant:14.5266 μM			
Number of hydrogen bonding: 6			Number of hydrogen bonding: 4			Number of hydrogen bonding: 3			

physicochemical properties of 2245 drugs in the World Drug Index (WDI) database approved for Phase II clinical studies (Lipinski et al., 1997). If we summarize these rules as follows:

- $\text{MlogP} \leq 5$;
- Molecular weight (MW) ≤ 500 g/mol;
- Number of H-bond acceptor (HBA) ≤ 10 and number of H-bond donors (HBD) ≤ 5 ;
- Number of rotatable bonds (n_{Rot}) ≤ 10 ;
- Topological Polar Surface Area (TPSA) $< 140 \text{ \AA}^2$.

In this section, the pharmacokinetic parameters of **Ata1-9** were obtained and tabulated as in Table S5 in accordance with the criteria defined above. These parameters were obtained with the help of SwissADME web page (<http://www.swissadme.ch/>). In addition, bioavailability radars and predicted Boiled Egg plot were created by taking these rules into consideration and are shown in Figures 10 and 11, respectively. According to the obtained results, the synthesized **Ata1-9** compounds meet these criteria in other words as can be seen the theoretical ADME results of the synthesized compounds (except **Ata1**, **Ata2**, **Ata4**, **Ata5**, **Ata7** and **Ata8** molecular weights in these compounds fall outside the

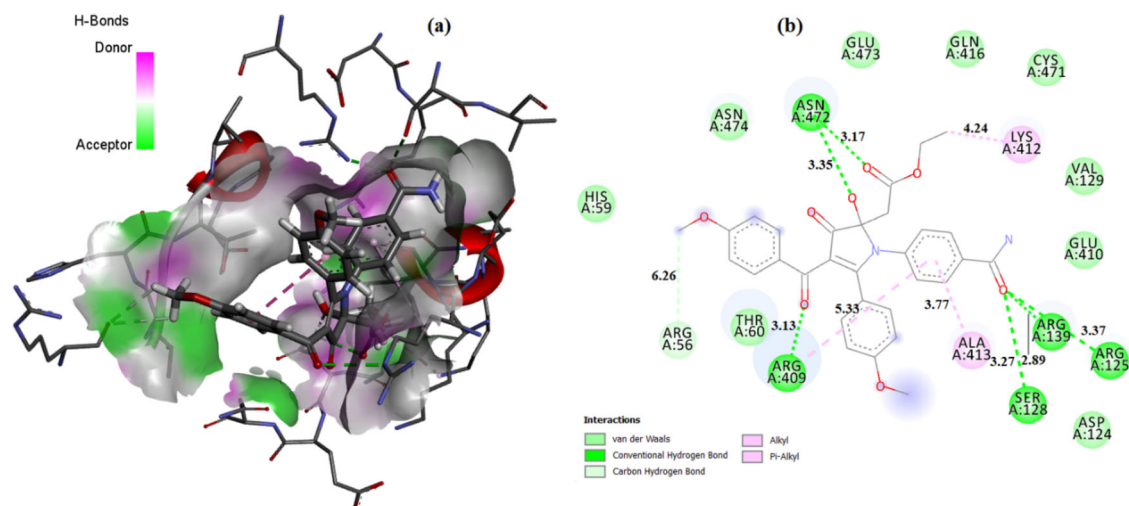
reference range) are in agreement with the five rule of Lipinski. Cytochromes P450 (CYP) are enzymes that play an important role in the breakdown of drugs to be excreted from the body (Hollenberg, 2002). Their inhibition causes a delay in the excretion of drugs from the body (Kirchmair et al., 2015). The five main enzymes of this system (CYP1A2, CYP2C19, CYP2C9, CYP2D6 and CYP3A4) play an important role in rendering harmless therapeutic molecules. According to the conducted study as *in silico*, the potentials of **Ata1-9** molecules to affect these enzyme activities were presented in Table S5. From these results, we can say that the synthesized compounds have no potential to affect the activities of these enzymes. From the Table S5 aqueous solubility (Ali log S) values were obtained as ≤ 0 . As a result, we can say that target molecules (**Ata1-9**) possess a good pharmacokinetic profile.

4.9. Prediction of ADMET and related properties

In this section, AdmetSAR analysis of the **Ata1-9** compounds was performed with the help of AdmetSAR 2.0 web page (<http://lmmd.ecust.edu.cn/admetSar2/>) and the some important selected results were given as in Table S6. It is

Table 6. AutoDock Vina results of the binding affinity and RMSD values of different poses in CYP2H substrate/3TDA (A chain) protein inhibitor of the title compounds.

Mode	Ata1-3TDA (A chain)			Ata2-3TDA (A chain)			Ata3-3TDA (A chain)		
	affinity (kcal/mol)	rmsd l.b.	rmsd u.b.	affinity (kcal/mol)	rmsd l.b.	rmsd u.b.	affinity (kcal/mol)	rmsd l.b.	rmsd u.b.
1	-8.1	0.000	0.000	-7.7	0.000	0.000	-6.7	0.000	0.000
2	-8.0	1.347	2.371	-7.5	3.304	8.415	-6.5	3.050	8.060
3	-7.7	4.373	9.195	-7.1	3.313	8.941	-6.5	4.136	8.345
4	-7.6	3.459	6.810	-7.0	20.624	23.362	-6.5	2.598	3.660
5	-7.4	3.809	8.264	-6.8	3.170	6.308	-6.5	1.386	5.894
6	-7.1	3.517	8.660	-6.6	5.461	9.891	-6.5	4.966	8.816
7	-7.0	19.541	23.113	-6.3	39.813	42.822	-6.3	4.222	7.692
8	-6.9	22.606	26.256	-6.2	28.306	33.567	-6.3	4.092	8.213
9	-6.9	5.150	10.651	-5.9	29.196	33.597	-6.0	3.534	5.805
10	-6.7	18.914	22.159	-5.8	31.175	35.819	-5.9	1.877	6.104
Inhibition constant:1.1552 μM			Inhibition constant:2.26913 μM			Inhibition constant:12.2706 μM			
Number of hydrogen bonding: 1			Number of hydrogen bonding: 2			Number of hydrogen bonding: 2			
Mode	Ata4-3TDA (A chain)			Ata5-3TDA (A chain)			Ata6-3TDA (A chain)		
	affinity (kcal/mol)	rmsd l.b.	rmsd u.b.	affinity (kcal/mol)	rmsd l.b.	rmsd u.b.	affinity (kcal/mol)	rmsd l.b.	rmsd u.b.
1	-7.1	0.000	0.000	-7.1	0.000	0.000	-6.8	0.000	0.000
2	-7.1	2.755	6.509	-7.1	2.758	6.103	-6.6	2.808	3.837
3	-7.0	2.984	5.340	-7.0	2.808	5.753	-6.4	2.445	5.176
4	-6.8	5.215	8.285	-6.7	5.507	8.549	-6.1	16.483	18.957
5	-6.8	3.832	7.669	-6.6	15.911	18.671	-6.0	5.269	8.062
6	-6.3	28.437	32.518	-6.3	16.734	19.810	-6.0	38.348	41.362
7	-6.0	9.291	14.951	-6.3	7.896	11.021	-5.9	5.381	8.070
8	-6.0	17.990	21.973	-6.2	16.398	18.660	-5.8	16.755	19.384
9	-5.9	28.043	32.615	-6.2	22.245	24.871	-5.7	15.323	19.043
10	-5.8	15.805	20.044	-6.1	17.133	18.763	-5.7	33.114	36.650
Inhibition constant:6.24687 μM			Inhibition constant:6.24687 μM			Inhibition constant:10.3649 μM			
Number of hydrogen bonding: 1			Number of hydrogen bonding: 1			Number of hydrogen bonding: 0			
Mode	Ata7-3TDA (A chain)			Ata8-3TDA (A chain)			Ata9-3TDA (A chain)		
	affinity (kcal/mol)	rmsd l.b.	rmsd u.b.	affinity (kcal/mol)	rmsd l.b.	rmsd u.b.	affinity (kcal/mol)	rmsd l.b.	rmsd u.b.
1	-7.3	0.000	0.000	-7.3	0.000	0.000	-6.7	0.000	0.000
2	-7.2	3.203	6.140	-7.2	2.698	9.024	-6.3	33.795	35.791
3	-7.0	3.560	7.110	-7.1	3.446	7.937	-6.1	26.430	29.614
4	-6.8	16.618	23.224	-7.0	21.230	25.207	-5.9	33.746	38.243
5	-6.3	34.486	37.752	-6.9	3.103	7.704	-5.9	34.774	38.341
6	-6.2	22.972	25.230	-6.6	6.586	11.298	-5.8	25.447	28.753
7	-6.2	24.043	26.167	-6.3	26.523	31.900	-5.7	29.512	32.563
8	-6.2	16.449	22.864	-6.2	41.976	45.105	-5.7	1.869	2.332
9	-6.1	17.025	22.062	-6.2	4.697	8.699	-5.4	30.923	34.608
10	-6.0	35.168	39.533	-6.2	35.962	39.692	-5.3	8.329	11.281
Inhibition constant:4.45719 μM			Inhibition constant:4.45719 μM			Inhibition constant:12.2706 μM			
Number of hydrogen bonding: 3			Number of hydrogen bonding: 2			Number of hydrogen bonding: 6			

**Figure 8.** (a) 3D and (b) 2D molecular docking results of the *Ata-7* for PDB: 3RZE.

determined that all the compounds indicate negative response for blood–brain barrier (BBB) criteria, but *Ata5* molecule indicates positive response. This output shows us that the *Ata5* molecule can pass the BBB. All the compounds indicate III category acute oral toxicity; therefore, it can be predicted that these molecules are relatively harmless for

oral administration, and all compounds are non-carcinogenic. From the Table S6, it is determined that *Ata1*, *Ata2*, *Ata3*, *Ata4*, *Ata5* and *Ata6* compounds indicate inhibitor effect for P-glycoprotein, but *Ata7*, *Ata8* and *Ata9* molecules indicate non-inhibitor effect. In line with the information obtained from the literature (Amin, 2013), we can say that the

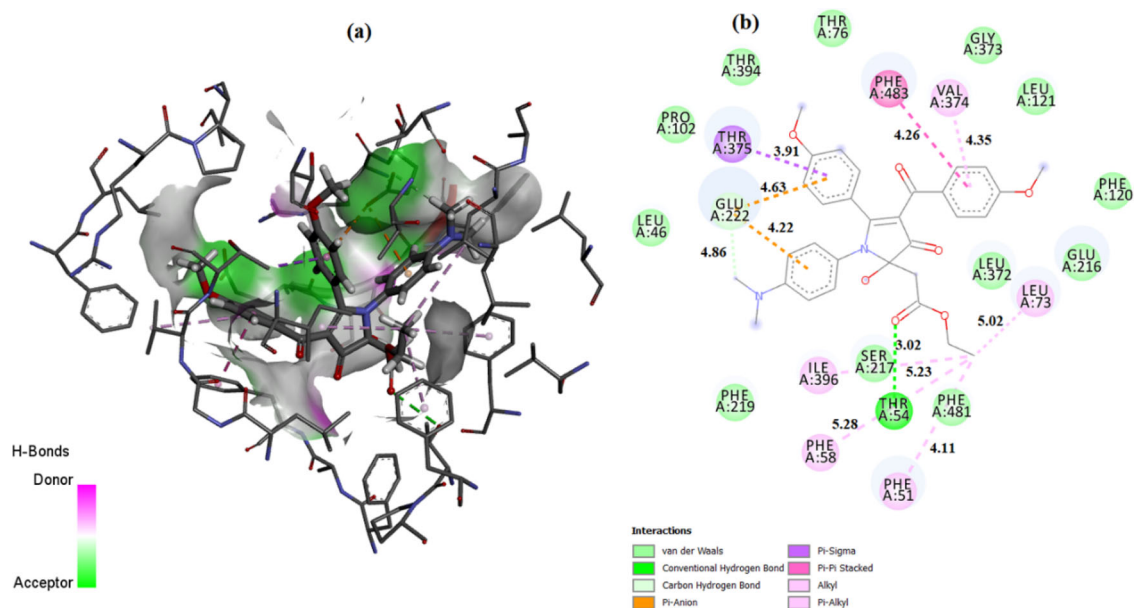


Figure 9. (a) 3D and (b) 2D molecular docking results of the Ata-1 for PDB: 3TDA (A chain).

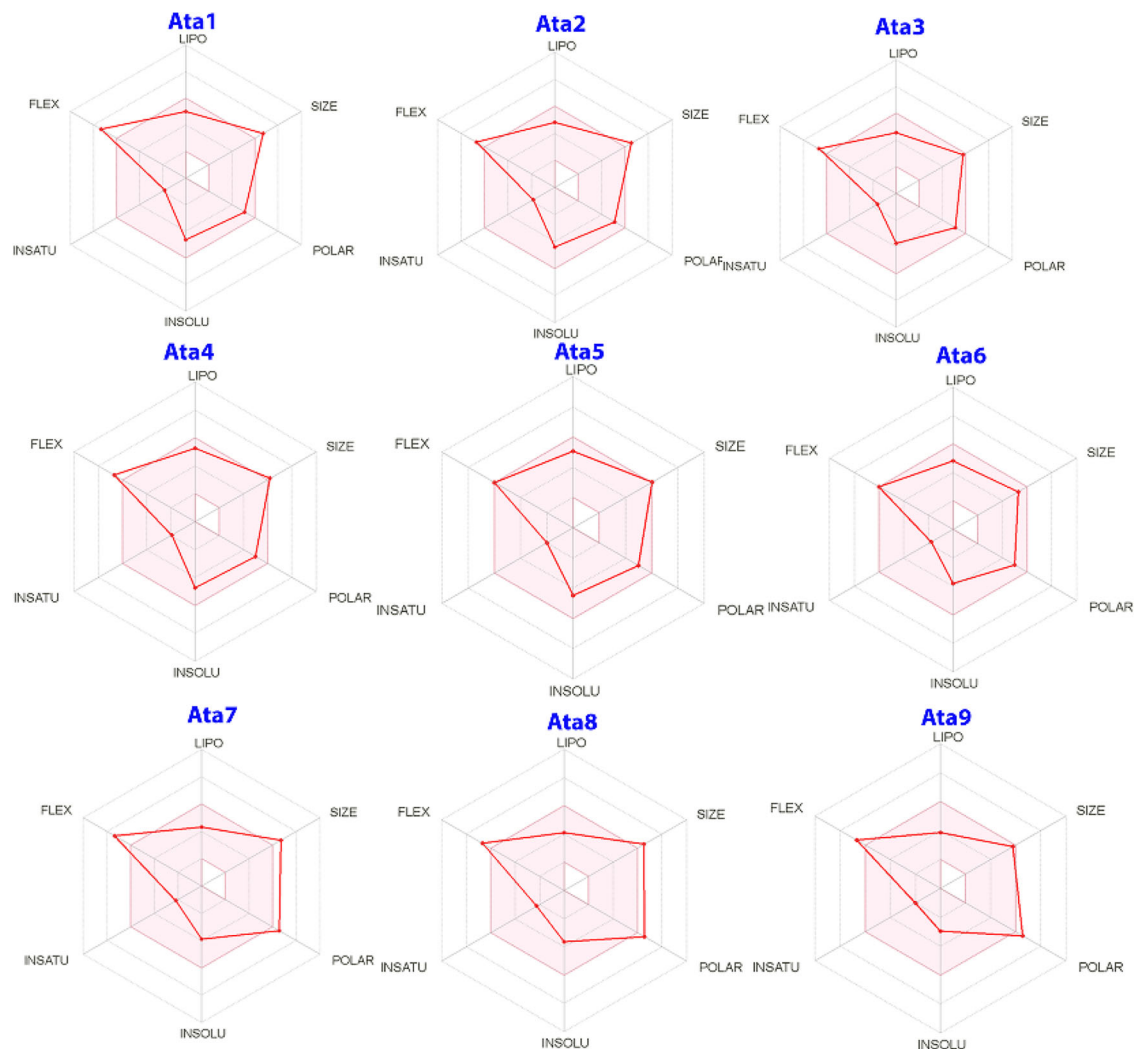


Figure 10. The bioavailability radars for the analyzed compounds.

inhibition of P-glycoprotein can prevent the absorption, permeability and retention of the compounds or drugs. On the other hand, all compounds indicate weak inhibitor

property for human ether-a-go-go-related gene (hERG). Finally, human intestinal absorption values were obtained positive for all compounds.

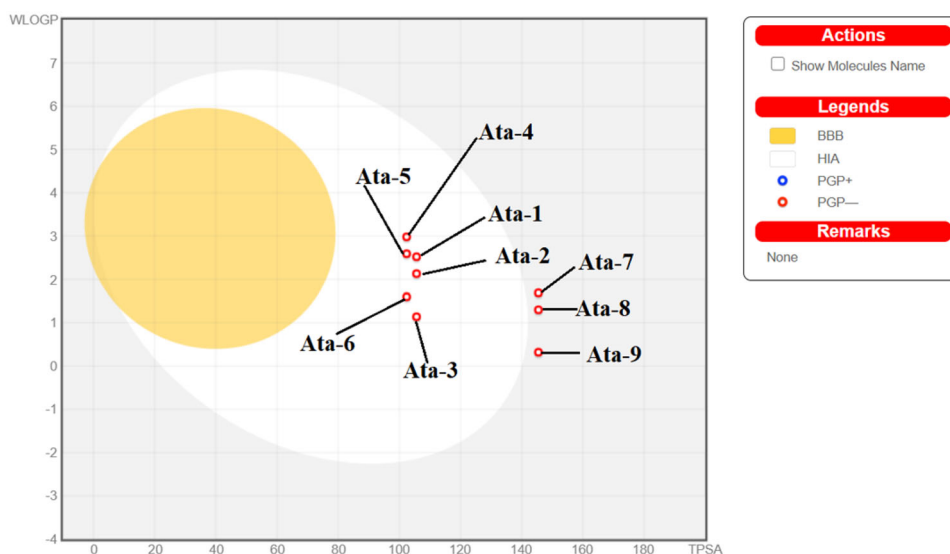


Figure 11. Boiled-Egg model of **Ata1-9** compounds.

5. Conclusions

In summary, nine novel pyrrol-3-one derivatives were successfully synthesized, and their structures were characterized by FT-IR, ^1H NMR, ^{13}C NMR and HRMS techniques. The produced organic samples' experimental dielectric properties showed that **Ata1** and **Ata3** have different dielectric properties. It was observed that **Ata1** has negative dielectric values at a relatively high-frequency range. This observation may be related to electron-donating and electron-accepting groups in the molecule structure. To support experimental spectroscopic results (NMR and UV), the theoretical calculations were carried out with the DFT-B3LYP/6-311++G(d,p) model-method/level for **Ata1-9** compounds. Over the optimized structures within the DMF solvent HOMO and LUMO distributions were obtained the theoretical UV results were supported and the theoretical results were found to be consistent with the experimental data. With the help of MEP analysis, the electrophilic and nucleophilic attack points on the **Ata1-9** molecules were determined and analyzed. From the NLO results, we can say that as a consequence the first-order hyper-polarizability values of pyrroles containing amide group were found to be high. Later, antieczematic and CYP2H substrate properties of the **Ata1-9** molecule were researched with the help of online PASS analysis and Autodock Vina program. These results concluded that the compounds are potent inhibitor for antieczematic/3RZE and CYP2H substrate/3TDA (A chain). When the MEP diagrams of the studied ligands were examined, it was observed that the electron-rich regions were on oxygen atoms. In molecular docking studies, ligands formed hydrogen bonds by bonding to proteins from these regions, which were also observed in MEP diagrams. Finally, from drug-Likeness, physicochemical and ADME/T results show that **Ata1-9** compounds were found to have good pharmacokinetic profile.

Disclosure statement

All authors declare that they have no conflict of interests.

Author contributions

All authors have made essential contributions to this study. Establishing the outline of the study: İK, YS; synthesis and characterization: İÇ, MG, İK; dielectric spectroscopy experiments: HÇ; theoretical and molecular docking studies: YS, HG; manuscript drafting; İK, YS, HÇ. All authors read and approved the final manuscript.

Funding

The authors would like to thank Science and Technology Practice & Research Centre of Bozok University for financial support (Project No: 6602c-SMYO/20-357).

ORCID

İrfan Çapan <http://orcid.org/0000-0002-9555-1555>
 Mehmet Gümüş <http://orcid.org/0000-0001-9262-7940>
 Halil Gökçe <http://orcid.org/0000-0003-2258-859X>
 Hidayet Çetin <http://orcid.org/0000-0002-8373-6990>
 Yusuf Sert <http://orcid.org/0000-0001-8836-8667>
 İrfan Koca <http://orcid.org/0000-0001-7873-159X>

References

- Aksu, K., Özgeriş, B., & Tümer, F. (2019). Synthesis and -characterization of new N-substituted 2-aminopyrrole derivatives. *Organic Communications*, 12, 38–42.
- Amin, M. L. (2013). P-glycoprotein inhibition for optimal drug delivery. *Drug Target Insights*, 7, DTI. S12519. <https://doi.org/10.4137/DTI.S12519>
- Berman, H. M., Henrick, K., Nakamura, H. (2003). Announcing the worldwide Protein Data Bank, *Nature Structural Biology*, 10(12), 980.
- Bhardwaj, V., Gumber, D., Abbot, V., Dhiman, S., & Sharma, P. (2015). Pyrrole: A resourceful small molecule in key medicinal hetero-aromatics. *RSC Advances*, 5(20), 15233–15266. <https://doi.org/10.1039/C4RA15710A>
- Dassault Systèmes BIOVIA, Discovery Studio Modeling Environment, Release 2017, San Diego: Dassault Systèmes, 2016. <http://www.3dsbiovia.com>
- Daina, A., Michielin, O., Zoete, V. (2017). SwissADME: A free web tool to evaluate pharmacokinetics, drug-likeness and medicinal chemistry friendliness of small molecules. *Scientific Reports*, 7, 42717.

- de Lima, W. E. A., Francisco, A., da Cunha, E. F., Radic, Z., Taylor, P., França, T. C., & Ramalho, T. C. (2017). Mechanistic studies of new oximes reactivators of human butyryl cholinesterase inhibited by cyclosarin and sarin. *Journal of Biomolecular Structure & Dynamics*, 35(6), 1272–1282. <https://doi.org/10.1080/07391102.2016.1178173>
- Ea de Lima, W., F Pereira, A., A de Castro, A., Ff da Cunha, E., & C Ramalho, T. (2016). Flexibility in the molecular design of acetylcholinesterase reactivators: Probing representative conformations by chemometric techniques and docking/QM calculations. *Letters in Drug Design & Discovery*, 13, 360–371.
- Filimonov, D., Lagunin, A., Glorizova, T., Rudik, A., Druzhilovskii, D., Pogodin, P., & Poroikov, V. (2014). Prediction of the biological activity spectra of organic compounds using the PASS online web resource. *Chemistry of Heterocyclic Compounds*, 50(3), 444–457. <https://doi.org/10.1007/s10593-014-1496-1>
- Filimonov, D. A., Lagunin, A. A., Glorizova, T. A., Rudik, A. V., Druzhilovskii, D. S., Pogodin, P. V., Poroikov, V. V. (2014). Prediction of the biological activity spectra of organic compounds using the PASS online web resource. *Chemistry of Heterocyclic Compounds*, 50(3), 444–457.
- Frisch, M. J. (2009). Gaussian 09, Revision D. 01. Gaussian Inc.
- Fukui, K. (1982). Role of frontier orbitals in chemical reactions. *Science (New York, N.Y.)*, 218(4574), 747–754. <https://doi.org/10.1126/science.218.4574.747>
- Geerlings, P., De Proft, F., & Langenaeker, W. (2003). Conceptual density functional theory. *Chemical Reviews*, 103(5), 1793–1874. <https://doi.org/10.1021/cr990029p>
- Gholap, S. S. (2016). Pyrrole: An emerging scaffold for construction of valuable therapeutic agents. *European Journal of Medicinal Chemistry*, 110, 13–31. <https://doi.org/10.1016/j.ejmech.2015.12.017>
- Gümüş, M., Sert, Y., Yalkın, A., Gökce, H., & Koca, İ. (2019). Synthesis, experimental and theoretical characterization of novel pyrimidine-5-carboxamides. *ChemistrySelect*, 4(16), 4695–4708. <https://doi.org/10.1002/slct.201900780>
- Hinchliffe, A., & Soscún M, H. J. (1994). Ab initio studies of the dipole polarizabilities of conjugated molecules: Part 2. *Journal of Molecular Structure: Theochem*, 304(2), 109–120. [https://doi.org/10.1016/S0166-1280\(96\)80003-0](https://doi.org/10.1016/S0166-1280(96)80003-0)
- Hollenberg, P. F. (2002). Characteristics and common properties of inhibitors, inducers, and activators of CYP enzymes. *Drug Metabolism Reviews*, 34(1–2), 17–35. <https://doi.org/10.1081/dmr-120001387>
- Kirchmair, J., Göller, A. H., Lang, D., Kunze, J., Testa, B., Wilson, I. D., Glen, R. C., & Schneider, G. (2015). Predicting drug metabolism: Experiment and/or computation? *Nature Reviews. Drug Discovery*, 14(6), 387–404. <https://doi.org/10.1038/nrd4581>
- Koca, İ., Saçmacı, M., Yılmaz, F., & Üngören, ŞH. (2014). Synthesis and structural characterization of pyrrole heterocyclic systems bearing amino acid units: Novel pyrrol-3-ones, pyrrolo [1, 2-a][3, 1] benzoxazines, and pyrrolo [2, 1-b][1, 3] oxazoles. *Journal of Heterocyclic Chemistry*, 51(1), 212–218. <https://doi.org/10.1002/jhet.1509>
- Koca, İ., Yiğitcan, S., Gümüş, M., Gökce, H., & Sert, Y. (2020). A new series of sulfa drugs containing pyrazolyl acylthiourea moiety: Synthesis, experimental and theoretical spectral characterization and molecular docking studies. *Journal of Molecular Structure*, 1204, 127479. <https://doi.org/10.1016/j.molstruc.2019.127479>
- Koca, İ., & Yildirim, I. (2012). Synthesis and spectroscopic characterization of pyrrole-2, 3-diones and their following reactions with 1, 2-aromatic diamines. *Organic Communications*, 5, 135.
- Kremer, F., & Schönhal, A. (2002). *Broadband dielectric spectroscopy*. Springer Science & Business Media.
- Kuca, K., Musilek, K., Jun, D., Zdarova-Karasova, J., Nepovimova, E., Soukup, O., Hrabínova, M., Mikler, J., Franca, T. C. C., Da Cunha, E. F. F., De Castro, A. A., Valis, M., & Ramalho, T. C. (2018). A newly developed oxime K203 is the most effective reactivator of tabun-inhibited acetylcholinesterase. *BMC Pharmacology and Toxicology*, 19(1), 1–10. <https://doi.org/10.1186/s40360-018-0196-3>
- Li, B., Sui, G., & Zhong, W. H. (2009). Single negative metamaterials in unstructured polymer nanocomposites toward selectable and controllable negative permittivity. *Advanced Materials*, 21(41), 4176–4180. <https://doi.org/10.1002/adma.200900653>
- Lipinski, C. A., Lombardo, F., Dominy, B. W., & Feeney, P. J. (1997). Experimental and computational approaches to estimate solubility and permeability in drug discovery and development settings. *Advanced Drug Delivery Reviews*, 23(1–3), 3–25. [https://doi.org/10.1016/S0169-409X\(96\)00423-1](https://doi.org/10.1016/S0169-409X(96)00423-1)
- Luque, F. J., López, J. M., & Orozco, M. (2000). Perspective on “Electrostatic interactions of a solute with a continuum. A direct utilization of ab initio molecular potentials for the prevision of solvent effects. *Theoretical Chemistry Accounts*, 103(3–4), 343–345. <https://doi.org/10.1007/s002149900013>
- Maxwell, J. C. (1892). *A Treatise on Electricity and Magnetism*. Clarendon.
- O’boyle, N. M., Tenderholt, A. L., & Langner, K. M. (2008). Cclib: A library for package-independent computational chemistry algorithms. *Journal of Computational Chemistry*, 29(5), 839–845. <https://doi.org/10.1002/jcc.20823>
- Parr, R. G., & Pearson, R. G. (1983). Absolute hardness: Companion parameter to absolute electronegativity. *Journal of the American Chemical Society*, 105(26), 7512–7516. <https://doi.org/10.1021/ja00364a005>
- Pearson, R. G. (1986). Absolute electronegativity and hardness correlated with molecular orbital theory. *Proceedings of the National Academy of Sciences of the United States of America*, 83(22), 8440–8441. <https://doi.org/10.1073/pnas.83.22.8440>
- Qin, M., Tian, Y., Han, X., Cao, Q., Zheng, S., Liu, C., Wu, X., Liu, L., Meng, Y., Wang, X., Zhang, H., & Hou, Y. (2020). Structural modifications of indolinones bearing a pyrrole moiety and discovery of a multi-kinase inhibitor with potent antitumor activity. *Bioorganic & Medicinal Chemistry*, 28(11), 115486. <https://doi.org/10.1016/j.bmc.2020.115486>
- Ramasamy, R. P., Yang, K., & Rafailovich, M. H. (2014). Polypropylene-graphene—a nanocomposite that can be converted into a meta-material at desired frequencies. *RSC Advances*, 4(85), 44888–44895. <https://doi.org/10.1039/C4RA05814C>
- Saçmacı, M., Üngören, Ş., & Akçamur, Y. (2006). Preparation and characterization of novel pyrrol-3-ones attached to alpha/beta-amino acids, esters and amides. *Amino Acids*, 31(4), 397–401. <https://doi.org/10.1007/s00726-006-0340-z>
- Saçmacı, M., Üngören, Ş. H., Akçamur, Y., Arıcı, C., & Ülkü, D. (2005). 2, 4, 5-Substituted furan-3 (2H)-ones: Synthesis, reactions with amino acid and hydrazine derivatives. *Heteroatom Chemistry*, 16(3), 235–241. <https://doi.org/10.1002/hc.20115>
- Saçmacı, M., Bolukbası, H., & Sahin, E. (2012). Reactions of some furan-3-ones with 2, 3-diaminopyridine and its derivatives. *Bulletin of the Korean Chemical Society*, 33(1), 90–94. <https://doi.org/10.5012/bkcs.2012.33.1.90>
- Scrocco, E., & Tomasi, J. (1973). *Topics in current chemistry*. New Concepts II.
- Trott, O., & Olson, A. J. (2010). AutoDock Vina: Improving the speed and accuracy of docking with a new scoring function, efficient optimization, and multithreading. *Journal of Computational Chemistry*, 31(2), 455–461. <https://doi.org/10.1002/jcc.21334>
- Üngören, Ş., Saçmacı, M., Akçamur, Y., Arıcı, C., & Ülkü, D. (2004). Synthesis of new 2, 3-dihydrofuran-3-one derivative and its reactions with some primary amines. *Journal of Heterocyclic Chemistry*, 41(2), 151–155. <https://doi.org/10.1002/jhet.5570410203>
- Vengatesh, G., Sundaravadivelu, M., & Muthusubramanian, S. (2020). Iodine mediated rearrangement of tetraarylpiperidin-4-ones: Synthesis, structure analysis and biological studies of 5-aryl-2-methoxy-2, 4-diphenyl-1H-pyrrole-3-ones. *Journal of Molecular Structure*, 1199, 126980. <https://doi.org/10.1016/j.molstruc.2019.126980>
- Verbiest, T., Houbrechts, S., Kauranen, M., Clays, K., & Persoons, A. (1997). Second-order nonlinear optical materials: Recent advances in chromophore design. *Journal of Materials Chemistry*, 7(11), 2175–2189. <https://doi.org/10.1039/a703434b>
- Wang, X., & Cai, C. (2012). A possible mechanism for the negative capacitance observed in organic devices. *arXiv Preprint arXiv:12107904*.
- Wolff, J. J., & Wortmann, R. (1999). Organic materials for second-order non-linear optics. In: *Advances in physical organic chemistry* (vol. 32, pp. 121–217). Elsevier.
- Yang, H., Lou, C., Sun, L., Li, J., Cai, Y., Wang, Z., Li, W., Liu, G., Tang, Y., (2018) admetSAR 2.0: Web-service for prediction and optimization of

- chemical ADMET properties. *Bioinformatics*, bty707. <http://lmm.d.ecust.edu.cn/admetsar2>
- Yan, H., Zhao, C., Wang, K., Deng, L., Ma, M., & Xu, G. (2013). Negative dielectric constant manifested by static electricity. *Applied Physics Letters*, 102(6), 062904. <https://doi.org/10.1063/1.4792064>
- Zhan, C.-G., Nichols, J. A., & Dixon, D. A. (2003). Ionization potential, electron affinity, electronegativity, hardness, and electron excitation energy: Molecular properties from density functional theory orbital energies. *The Journal of Physical Chemistry A*, 107(20), 4184–4195. <https://doi.org/10.1021/jp0225774>